CrossMark

INVITED FEATURE PAPER

Epitaxial lanthanide oxide thin films on Si for high-*k* gate dielectric application: Growth optimization and defect passivation

Ayan Roy Chaudhuri[a)]
Materials Science Centre, Indian Institute of Technology, Kharagpur 721302, India

Andrea Fissel and Hans Jörg Osten
Institute of Electronic Materials and Devices, Leibniz University Hannover, D-30167 Hannover, Germany

(Received 31 August 2016; accepted 4 January 2017)

Epitaxial layers of insulating binary lanthanide oxides have been considered as potential alternative to conventional SiO_2 for gate dielectric application in future Si-based MOSFET devices, which was investigated in more detail for epitaxial Gd_2O_3 and Nd_2O_3 as model systems. Additionally, the ability to integrate epitaxial dielectric barrier layers into Si structures can usher also in a variety of novel applications involving oxide/silicon/oxide heterostructures in diverse nanoelectronic and quantum-effect devices. Although epitaxial layers of such ionic oxides with excellent structural quality can be grown using molecular beam epitaxy, they often exhibit poor electrical properties such as high leakage current density, flat band instability, poor reliability etc. owing to the presence of electrically active charge defects, generated either during the oxide layer growth or typical subsequent CMOS process steps. Based on the origin and individual character of these defects, we review various aspects of defect prevention and passivation which lead to a significant improvement in the dielectric properties of the heterostructures.

I. INTRODUCTION

The physical dimension of metal oxide field effect transistors (MOSFETs) which are essential components of semiconductor integrated circuits (ICs) have been subjected to continuous downscaling since the birth of ICs to improve the device performance and reduce the production cost per bit. This shrinking of the semiconductor device dimension follows an empirical trend popularly known as Moore's law, which describes that the number of transistors per IC, or in other words processing capacity and speed doubles, every two years.[1] Moore's prediction was found true for a long while thanks to the rapid advancement of semiconductor device processing technologies such as lithography, selective etching processes etc. On the other hand from the materials aspect, the key material property that enabled the existence of Si-MOSFET devices is the excellent insulating characteristic of SiO_2 thin layers which is used as the gate dielectric to isolate the transistor gate from the Si channel. This is possible due to the large band gap of SiO_2 (E_g ~9 eV), and the low density of interface traps with Si. For example, in advanced integrated devices SiO_2 gate dielectrics with charge densities of 10^{10} cm^{-2}, midgap interface state densities of 10^{10} cm^{-2}, and dielectric strength of 15 kV/cm have been produced.[2,3] Further, high quality layer of SiO_2 can be grown by simple thermal oxidation that remains amorphous at typical CMOS process condition which is less prone to any structural defects. However, it was evident that continuing the device scaling as per Moore's law cannot be pushed longer if SiO_2 has to be used further as the gate dielectric. The primary disadvantage of using SiO_2 as the gate dielectric is its relatively low dielectric constant (k ~3.9). This imposes significant reduction in the thickness of the SiO_2 layer as a consequence of downscaling the MOSFET devices to achieve higher gate capacitance necessary to produce the required drive current in submicron MOSFETs. For example, the specific gate capacitance used for todays CMOS technology nodes demands SiO_2 thickness <1 nm. Unfortunately, such ultrathin layers of SiO_2 cannot act really as an insulator, as direct tunneling through the dielectric barrier dominates the conduction behavior and the leakage current increases exponentially with decreasing gate dielectric layer thickness.[4] For example, scaling of the gate oxide below 1 nm leads to leakage current density of ~10 A/cm^2 at 1 V which is beyond the acceptable limit for low power device applications. It has also been demonstrated that fabricating CMOS devices with SiO_2 layer thickness in the range of 1.0–1.2 nm does not lead to any further gain in the drive current setting a fundamental limit for gate oxide scaling.[5] Moreover, in contrast to high performance microprocessors, the leakage current densities of transistors in case of low power consumption devices should be well below 10^{-1} A/cm^2,[6] making the gate oxide thickness

Contributing Editor: Don W. Shaw
a) Address all correspondence to this author.
e-mail: ayan@matsc.iitkgp.ernet.in
This paper has been selected as an Invited Feature Paper.
DOI: 10.1557/jmr.2017.22

Downloaded from https://www.cambridge.org/core. Technische Informationsbibliothek, on 05 Feb 2018 at 11:17:50, subject to the Cambridge Core terms of use, available at https://www.cambridge.org/core/terms. https://doi.org/10.1557/jmr.2017.22

issue more stringent. There have been additional limiting factors to SiO_2 scaling, such as boron diffusion from traditional highly doped poly-Si to lightly doped channel layer[7] that results in shift in the transistor threshold voltage and degraded device reliability owing to hot electron injection at the Si–SiO_2 interface causing dielectric breakdown of the gate oxide.[8] These issues related to material limited device scaling is most prominent in case of MOSFETs than in any other device components and became the showstopper in the historical progress of multibillion semiconductor industry.[2] In this context, one of the major challenge associated with further scaling of integrated devices was to find suitable replacement gate insulator material that possesses higher dielectric constant than SiO_2 and therefore can be grown with larger thickness which shall allow sufficient FET current drive while maintaining lower leakage current.[9]

II. CHOICE OF ALTERNATIVE GATE INSULATOR

SiO_2 is the key material that laid the foundation of Si based microelectronics technology and led it to flourish despite the average performance of Si compared to other semiconductors, such as Ge, GaAs, GaN, SiC, etc. which do not form a thermally stable native oxide. Integrating an alternative dielectric to Si would be possible only at the expense of the advantages of SiO_2, which makes the choice of alternative gate dielectric a critical issue. The semiconductor industry first found interim solution remaining within the Si-SiO_2 materials framework by selecting silicon oxynitride and oxide/nitride stacks as alternative gate dielectrics which offer slightly higher k value compared to SiO_2 and thus lead to reduced leakage, boron penetration, and reliability issues by using relatively larger gate dielectric layer thickness.[10] However, this was only a temporary solution as incorporation of increasing amount of N gives rise to side effects, such as severe degradation of electron mobility in the transistor channel and reduced band gap of the oxide.[8] Therefore, the search of really alternative dielectric materials with much higher dielectric constant was on the agenda to keep pace with the historical steep progress of Si technology. The first parameter to be considered for selecting an alternative material is the appropriate value of the dielectric constant that can be useful for transistor application. While leakage current through the dielectric layer in the direct tunnel regime depends exponentially on its thickness, the capacitance varies linearly. Consequently, dielectrics with too high dielectric constant lead to short channel performance degradation, owing to the fringing field from the gate to source/drain region due to large thickness to length aspect ratio of the gate dielectric.[11] Optimum k values within the range of 15 and 50 are predicted to be ideal for continuing scaling of transistors in the future, which shall be applicable for both low standby power and high performance devices.[9] Besides suitable higher k value, any material selected as alternative to substitute SiO_2 as gate dielectric will also have to satisfy several other criteria to be eligible for gate dielectric application, such as thermodynamic stability in direct contact with Si, thermal stability even at typical CMOS process temperatures of up to 1000 °C, large band gap, low bulk defect density, low interfacial trap densities, CMOS process compatibility and reliability.[2]

A wide variety of insulating metal oxides with much higher k values has been investigated in the past decade as viable alternative to Si-oxynitride and oxide/nitride systems. Many of these metal oxide alternative dielectrics appear to satisfy some of these requirements, but unfortunately only a very few materials are promising with respect to all of the guidelines. Furthermore, the process complexity associated with deposition of the high-k metal oxides in contrast to simple thermal deposition of SiO_2 and oxynitrides pose additional challenges for integrating the alternative dielectrics into mainstream Si technology, such as cost of the deposition tools for large scale production with proper stoichiometry and satisfactory microstructure control, in addition to the requirement of using metal gates, etching and related aspects.[12]

Different binary metal oxides have been considered promising because of the relative ease in controlling the stoichiometry in their thin films. But a number of these oxides are not stable in contact with Si at $T > 1000$ K and gives rise to an interfacial layer formation.[13] Interfacial layer exhibiting lower k value eventually leads to degradation of the effective dielectric constant and limits the scalability of the device. Another critical parameter to consider is the band gap of the metal oxides, which is mostly much smaller than that of SiO_2 ($\sim$9 eV), that directly influences their conduction band and valence band offset (VBO) energies with respect to Si. This is related to the ionic character of the metal oxides in contrast to covalent SiO_2. A number of representative dielectric oxides have been found to obey an approximate inverse relation between their static dielectric constant and band gap. This behavior is expected because stronger polarizability implies weaker bonding which leads to smaller separation in bonding and antibonding energies.[14] The band offsets, which determine the electron and hole injection barriers respectively at the oxide/Si interface, should be at least 1 eV (for both conduction and valence bands) to prevent charge carrier injection from Si into the bands of the chosen oxide.[15] Figure 1 illustrates the calculated band offsets of several promising high-k dielectric oxides with respect to Si. It is clearly evident that only a few of the high k oxides are suitable candidates for gate dielectric application, despite superior dielectric constant values of several other oxides.

An additional roadblock for integrating high-k metal oxides into Si technology is their lower crystallization

Downloaded from https://www.cambridge.org/core. Technische Informationsbibliothek, on 05 Mar 2018 at 11:20, subject to the Cambridge Core terms of use, available at https://www.cambridge.org/core/terms. https://doi.org/10.1557/jmr.2017.22

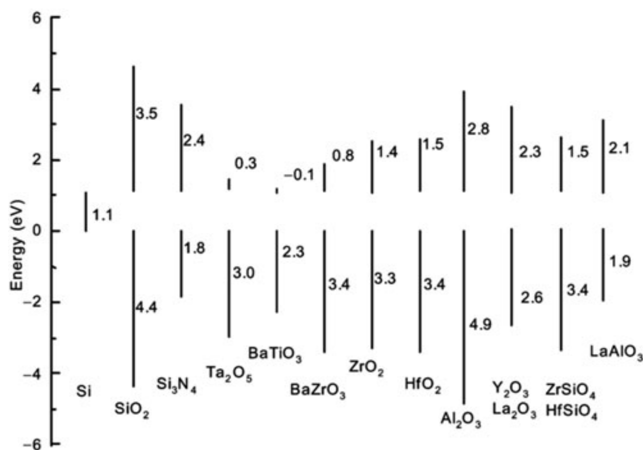

FIG. 1. Calculated conduction band and valence band offsets of various oxides on Si. (Reprinted with permission from Ref. 15. Copyright [2000], American Vacuum Society).

temperatures. Following the trend with SiO_2, the replacement gate dielectric is expected to involve amorphous metal oxides to avoid surface roughness and additional leakage due to the formation of grain boundaries as expected in crystalline material. The higher atomic coordination numbers and ionic character of the metal oxides render them poor glass formers.[16] Further, with increasing dielectric constant the crystallization temperature of the oxides also reduces due to increased ionicity, and even the recently preferred binary oxides (e.g., HfO_2, ZrO_2) do not withstand crystallization at typical CMOS processing temperatures. Alloying with Si or Al (i.e., silicates or aluminates) results in superior thermal stability and higher crystallization temperature,[12,17–19] however, again at the expense of the highest achievable dielectric constant.

Based on the dielectric performance and process condition optimization, the first generation of high-*k* dielectrics was expected to consist of Hf-based alloys. Interface engineering schemes have been developed to form oxynitride and oxide/nitride reaction barriers between these high-*k* oxides and Si to minimize the reaction at the interface.[20] The amorphous barrier layers used for Si surface passivation was not only promising for minimizing interfacial reaction but to maintain also high channel carrier mobility, which could otherwise be affected by the interfacial defects and the soft phonons of the high-*k* oxides in direct contact with Si. In 2007 Intel successfully demonstrated for the first time a 45 nm logic technology using Hf based high-*k* metal gate stack transistors in a high volume manufacturing process, where an equivalent oxide thickness (EOT) of ~1 nm was realized.[21] This has gained wide adoption in the industry.[6] While the integration of Hf based gate dielectric to the CMOS device process represented a remarkable success, it is obvious that the lowest possible EOT achievable using alternative dielectric material cannot be realized in presence of the interfacial layer due to their lower *k* values.

Therefore, clearly further downscaling of CMOS devices must involve usage of high-*k* oxide materials which should be integrated to Si without any interfacial layer to realize EOT <0.8 nm. Therefore, it is certainly not exaggeration to state that the quality of the interface between the high-*k* oxide and Si will be the most important parameter to impact the device performance. A good interface quality can be expected either if the oxide is amorphous so that the number of Si dangling bonds at the interface can be minimized by local bonding adjustment, or if it is lattice matched to Si and grown epitaxial with atomically sharp interface. Epitaxial grown high-*k* oxides could be a smart choice in this regard since this approach has the advantage of defined interface engineering and hence offers more control over the device properties despite larger process complexity related to the epitaxial growth process.

III. EPITAXIAL GATE INSULATORS: CHOICE OF ALTERNATIVE METAL OXIDES

In the recent past various epitaxial complex oxides, especially insulating binary rare earth oxides (REOs, mainly lanthanide oxides, LnOs), have drawn significant interest as prospective 2nd generation of alternative gate dielectrics.[22] Insulating LnOs form a very interesting group of materials for integration on Si[4] as they offer several advantages, such as large dielectric constant, large band gap and band offsets to Si, superior thermal and thermodynamic stabilities, which make them suitable for Si-based technologies.[13,22] However, the choice of appropriate LnOs for gate dielectric application depends strongly on their stoichiometry. For example, some rare-earth metals exhibit multiple oxidation states (+2, +3, and +4) which lead to oxides with different stoichiometry (LnO, Ln_2O_3, LnO_2),[23] where not all the compositions are insulating. Moreover, the position of the charge neutrality level of ionic oxides depends strongly on their stoichiometry.[24] Therefore, their band alignment to silicon and, finally, the leakage behavior becomes strongly dependent on the oxygen content. Therefore, LnOs which exhibit more than one stoichiometry (e.g., Ce-, Eu-oxides) or those which exhibits stable mixed valence structure (e.g., Pr_6O_{11}) are also not the best choices as alternative high-*k* materials in Si-based devices. Consequently, for practical application it is wise to focus on those insulating LnOs in which the Ln metal possesses only a single valence state. Based on these criteria we focused mainly on LnOs containing Ln^{3+} cations (exhibiting the composition Ln_2O_3).

Additionally, Ln_2O_3 oxides can occur in different crystal structural phases (polymorphs) depending on temperature, e.g., cubic bixbyite structure (Mn_2O_3 type),

Downloaded from https://www.cambridge.org/core. Technische Informationsbibliothek, on 05 Feb 2018 at 14:17:50, subject to the Cambridge Core terms of use, available at https://www.cambridge.org/core/terms. https://doi.org/10.1557/jmr.2017.22

hexagonal lanthanum oxide structure (La_2O_3 type), and monoclinic structure (Sm_2O_3 type). The different structures exhibit different dielectric properties. Since temperature-dependent crystal phase transitions are not reversible or not completely reversible, and accompanied by interfacial layer formation on Si, the controlled tuning of dielectric properties is difficult for Ln_2O_3s which can undergo structural phase transformation already within a temperature range typical for CMOS processing[25] which make them not suited for gate dielectric applications.

Based on these criteria we focus mainly on Gd_2O_3 (and to some extent on Nd_2O_3) for its epitaxial integration on Si as 2nd generation alternative high-*k* dielectric material. Bulk Gd_2O_3 occurs in the bixbyite cubic type of structure with single stoichiometry and structural transformation occurs only at $T > 1400$ K.[26] In addition, this oxide has a large band gap of about 6 eV and nearly symmetrical band offsets to Si,[27] a dielectric constant of 14 as well as a low lattice mismatch (~0.5%) with Si. The bixbyite structure of Gd_2O_3 has lattice symmetry suitable for epitaxial growth on Si(100) and Si(111). Although the lattice mismatch between Gd_2O_3 and Si are identical for (100)//(100), (110)//(110), and (111)//(111) epitaxial arrangements based on the symmetry matching, it is to be noted that in practice Gd_2O_3 grows with (111) orientation on Si(111), whereas (110) oriented growth of Gd_2O_3 is observed on Si(100) surface under usual epitaxial growth conditions. A detailed discussion of the impact of symmetry matching and surface energy criteria on the epitaxial relation for Gd_2O_3 growth on Si(100) can be found elsewhere.[22,28]

A. Epitaxial growth

The epitaxial layers of Gd_2O_3 on different Si surfaces were grown by evaporating commercially available stoichiometric granular Gd_2O_3 using electron gun in a cluster solid source cluster molecular beam epitaxy system that includes a growth, an annealing, and an analytic chamber connected by an ultra-high vacuum (UHV) transfer system. The layers were grown on silicon substrates with different orientations. Substrates were cleaned *ex situ* using the last step diluted HF etch followed by a dilution rinse, and then were immediately inserted into the vacuum system. Growth temperatures were in the range of 800–1000 K. Typical growth rates were 0.005–0.01 nm/s. For some growth experiments, additional molecular oxygen was inserted in the chamber without any activation to yield an oxygen partial pressure (P_{O_2}) in the range of 10^{-7} mbar. For the fabrication of metal electrodes, the wafers were transferred immediately after the growth *in vacuo* into another chamber, where metal dots were evaporated through a shadow mask using electron beam heating. The surface and layer structure was evaluated during the growth by reflection high-energy electron diffraction (RHEED). The chemical natures of the oxides and the band alignment with Si have been investigated using *in situ* X-ray photoelectron spectroscopy (XPS) in a separate chamber without exposing the layers to atmosphere. *Ex situ*, the layers were characterized by X-ray diffraction (XRD) (θ/2θ, ω and Φ-scans), by X-ray reflectivity for layer thickness determination (XRR) and by transmission electron microscopy (TEM). Figure 2 shows the X-ray (θ–2θ scan) diffraction patterns of Gd_2O_3 thin films grown on different Si substrates. The scan for Gd_2O_3 layer on Si(001) surface exhibits a distinct peak at 2θ = 46.4° corresponding to the *d*(440) inter planar spacing of cubic Gd_2O_3 along [110] orientation. The layers on the Si(111) substrate also exhibit single orientation without any indication of disoriented crystallites. The peaks at 28.5° and 59.4° corresponding to *d*(222) and *d*(444) interplanar spacing are hidden under the appropriate Si peaks. The scan for Gd_2O_3 thin films grown on Si(110) displays a peak at 28.5° confirming the preferential growth along (111) direction.

IV. DEFECTS IN EPITAXIAL HIGH-*k* RARE EARTH OXIDES: SELECTING OPTIMUM GROWTH CONDITION

The existence of various defects inside the layer and/or at the oxide/Si interface often degrades the device performance. Therefore, it is of paramount importance to understand the nature of the defects inside the metal-oxide stack and at the oxide/Si interface and address their effective passivation for successful integration of epitaxial LnOs to typical CMOS technology.

Defects in the epitaxial LnOs can be broadly classified into two categories, e.g., structural defects and charge defects. The structural defects include domain boundary, misfit dislocation, stacking faults etc., whereas the charge defect encompasses oxide fixed charge, mobile oxide charges, and interface traps. In the present article we shall

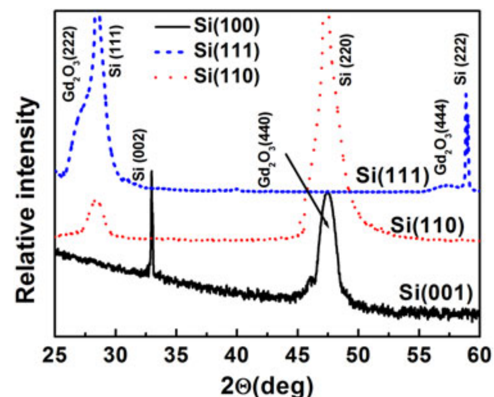

FIG. 2. X-ray diffraction patterns of Gd_2O_3 thin films grown on Si substrates with different orientation.

Downloaded from https://www.cambridge.org/core. Technische Informationsbibliothek, on 05 Feb 2018 at 14:17:50, subject to the Cambridge Core terms of use, available at https://www.cambridge.org/core/terms. https://doi.org/10.1557/jmr.2017.22

focus mainly on the charge defects normally encountered in the epitaxial LnOs, their effect on the electrical properties of these heterostructures, and their effective passivation. It should be noted that to understand the role of the charge defects in the LnO thin films it is necessary to realize good structural quality of the epitaxial layers and atomically sharp interfaces with Si. This is because in addition to the charge defects, the quality of interface between the oxide layer and Si surface also significantly influences the dielectric properties of the heterostructures. As a case study to understand the interface formation between the lanthanide oxides and Si, Fissel et al. reported a detailed investigation of the interface formation between Nd_2O_3 and Si(100) during epitaxial growth.[29] The RHEED investigation during MBE growth under UHV condition $\left(P_{O_2}<5\times10^{-8}\ \text{mbar}\right)$ revealed that during the initial stage of oxide layer deposition the surface reconstruction of Si(100) changes from usual (2 × 1) of a clean surface to an unreconstructed (1 × 1). Further deposition leads to additional fractional order RHEED spots appearing at the 1/3 positions between the main (0,1) spots of the zero order Laue zone corresponding to a 3-fold surface periodicity at the surface [Fig. 3(a)]. Similar observation was already reported for the epitaxial growth of Pr_2O_3 on Si(001).[30] During subsequent deposition, the surface changes back to the (1 × 1) structure before bulk spots appear related to diffraction from oxide islands [Fig. 3(b)]. The double spots in Fig. 3(b) correspond to two in-plane lattice constants nearly equal to the lattice constant of silicon and $\sqrt{2}$ times of that constant, respectively. This indicates that similar to other LnOs crystalline Nd_2O_3 grows in (110)-oriented domains, with orthogonal in-plane orientations.[22,31] This is also evident from the X-ray diffraction pattern in the θ–2θ geometry, where only the (440) diffraction peak from the oxide layer is visible for the growth on Si(100) (Fig. 4).

The Nd_2O_3/Si interface formation was investigated *in situ* by XPS at different stages of the oxide layer growth. For layers with a thickness in the range up to 1 nm, where the 3-fold periodicity in RHEED was found, the Si 2*p* core level binding energy mainly corresponds to elemental Si (Si^0 state) (Fig. 5). However, additionally a significant broadening was observed also toward the low-energy side of the Si^0 peak. Deconvolution of the spectra by Gaussian fit indicated that for layers with thickness ≤1 nm the broadening can be explained by the additional occurrence of a Si^{1-} bonding state due to the formation of Si–Nd bonds in the initial stage of growth. The relatively small shift in the peak position indicates the well-known $NdSi_2$ phase formation.[32] This finding agrees to an earlier report by Norton et al., where the formation of silicide like surface structure was also associated with the appearance of additional 1/3-order reflections on a (2 × 1) reconstructed surface during Sr deposition on Si(100).[33] With increase in the Nd_2O_3 layer thickness of above 1 nm the spectra exhibit additional peaks at higher binding energies which could be attributed to the different kinds of silicate like bonds.[34] The corresponding

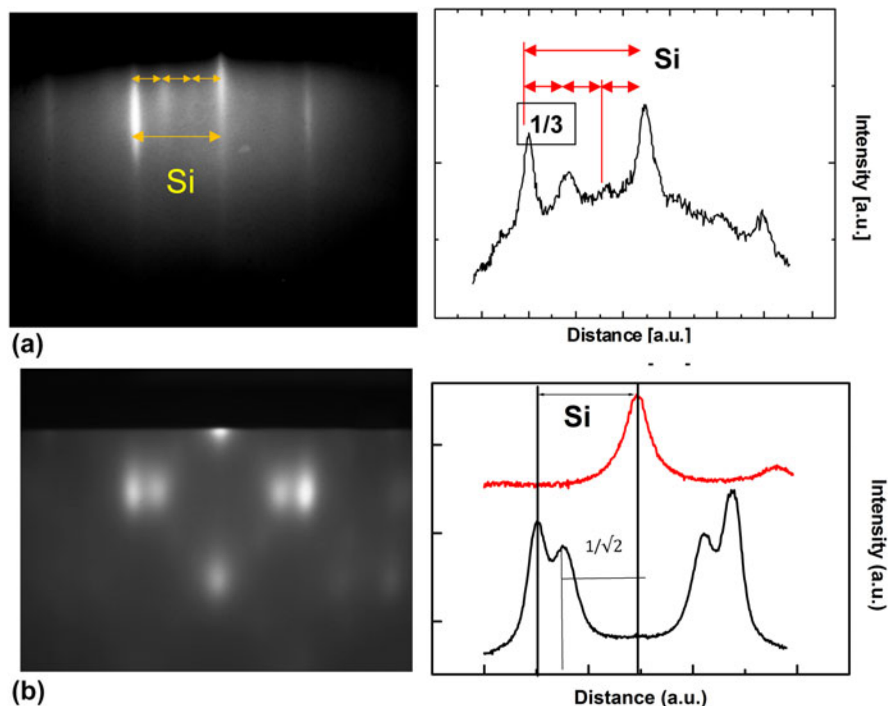

FIG. 3. RHEED pattern corresponding to Nd_2O_3 layer on a Si(100) wafer (a) 0.5 nm Nd_2O_3 and (b) 2 nm Nd_2O_3 layer thickness. The right hand side displays the intensity profiles along the marked line across the RHEED patterns.

Downloaded from https://www.cambridge.org/core. Technische Informationsbibliothek, on 05 Feb 2018 at 14:17:50, subject to the Cambridge Core terms of use, available at https://www.cambridge.org/core/terms. https://doi.org/10.1557/jmr.2017.22

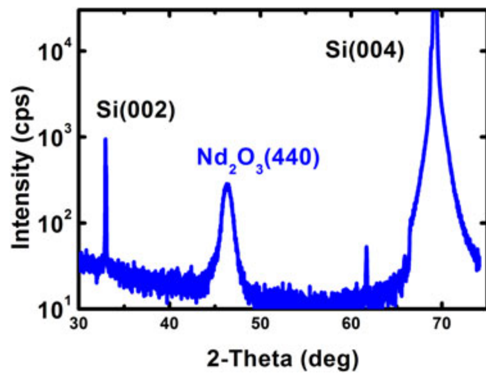

FIG. 4. X-ray diffraction pattern in the θ–2θ geometry of a 12 nm Nd_2O_3 layer grown on a Si (001) substrate.

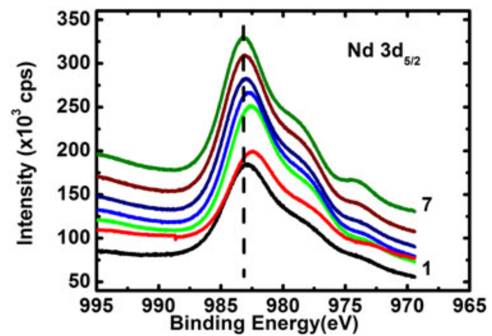

FIG. 6. Nd $3d_{5/2}$ core-level XPS spectra for Nd_2O_3 layers of various thicknesses ranging between 0.5 nm (Spectra 1) to 3 nm (spectra 7). The dashed line represents the expected peak position for bulk Nd_2O_3.

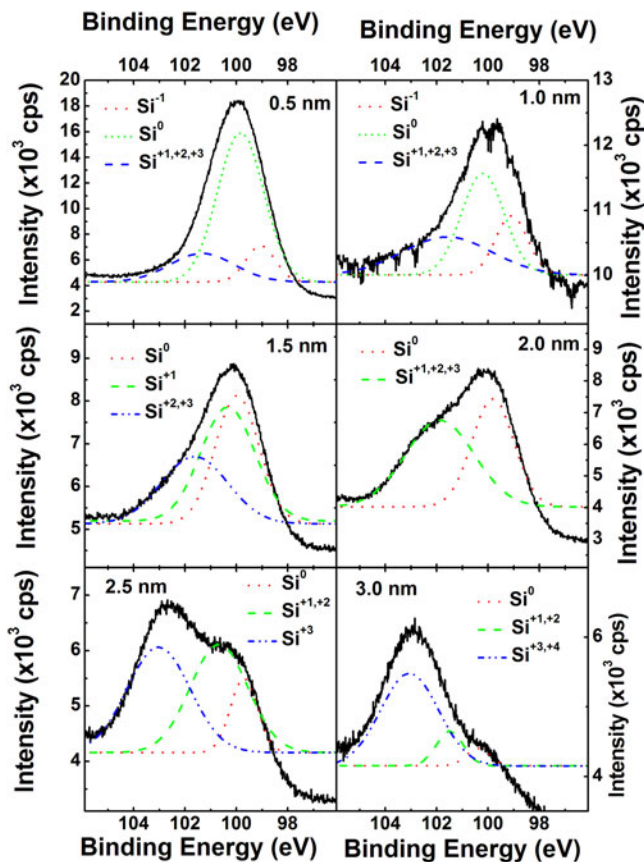

FIG. 5. Si $2p$ spectra together with the appropriate multi peak fitting results of a Si wafer at different stages of Nd_2O_3 layer growth.

neodymium $3d_{5/2}$ core-level spectra also supports the silicide-like bond formation at the interface during initial stage of the oxide layer growth (Fig. 6). For the second layer, a shift toward lower binding energies is observed which can be expected if the bonds become metal-like. That behavior together with the observed shifts in the Si spectra can only be explained by an exchange of oxygen bound to silicon by neodymium or by a movement of oxygen atoms from a Si–O–Nd interface site into the layer during the initial stage of growth. TEM investigations also support this assumption. Figure 7 shows TEM micrographs of an Nd_2O_3/Si(001) heterostructure grown under UHV conditions. The plan-view micrograph exhibits typical Moire fringes originating from interfacial inclusions [Fig. 7(a)]. The crystalline inclusion with the interface extending some nanometers into the Si substrates is clearly seen in the cross-sectional micrographs [Fig. 7(b)]. Additionally, voids were also found in such layers. Based on a detailed analysis of the TEM results, the crystallographic structure of these inclusions could be identified to be identical to the known structure of tetragonal $NdSi_2$.[35] Other LnOs deposited on Si under identical growth condition exhibits similar results. For LnOs growth, the formation and stability of the silicide-like phase depend on the oxygen chemical potential.[36] Considering the low P_{O_2} under UHV conditions (used in standard MBE growth), the chemical potential of oxygen can also become negative which can facilitate silicide formation over oxide formation. The silicide growth can continue as long as the oxygen chemical potential remains strongly negative due to low oxygen content. This effect predominates at a surface or interface region where the thermodynamic equilibrium is perturbed by different factors, such as stress.

However, such silicide inclusion at the Ln_2O_3/Si interface can potentially degrade their dielectric properties, especially in case of thin layers. Therefore, for high-k dielectric application the interfacial silicide inclusion has to be avoided. One possible means to circumvent the silicide inclusions is annealing the deposited layers in an oxygen-rich atmosphere. However, such post deposition annealing normally gives rise to an amorphous interfacial layer. Fissel et al. reported that such interfacial layer consists of two regions (Fig. 8), one with lighter and one with darker contrast which was attributed to two different silicates.[29]

These results indicate that to achieve a smooth interface between the epitaxial Ln_2O_3 and Si, further growth

Downloaded from https://www.cambridge.org/core. Technische Informationsbibliothek, on 05 Feb 2018 at 14:17:50, subject to the Cambridge Core terms of use, available at https://www.cambridge.org/core/terms. https://doi.org/10.1557/jmr.2017.22

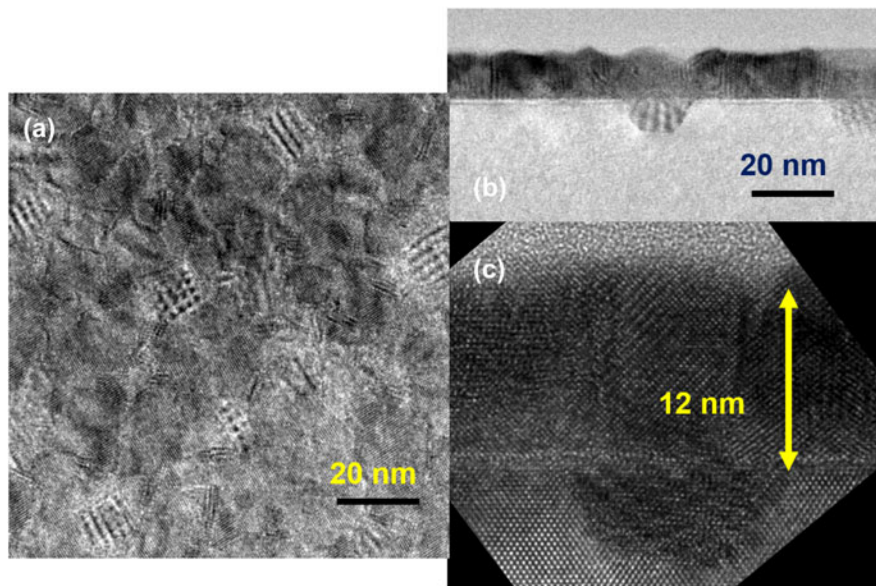

FIG. 7. TEM images of a Nd_2O_3 layer grown on Si(001), (a) plane-view micrograph, exhibiting pronounced Moiré fringes and (b, c) cross-sectional micrographs with different magnifications exhibiting the formation of crystalline interfacial inclusions. The two Nd_2O_3(110) domains are indicated by white lines parallel to the atomic planes.

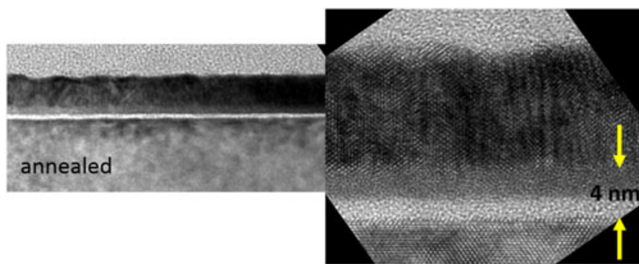

FIG. 8. Cross-sectional TEM micrograph of the Nd_2O_3 layer shown in Fig. 7, after annealing in nitrogen at a pressure of 2×10^{-2} mbar, and temperature if 600 °C for 10 min. In addition to the disappearance of the silicide inclusions, formation of an amorphous interfacial layer is visible.

engineering is necessary. In this view, a simple approach is to vary systematically the oxygen chemical potential by variation of the P_{O_2} during oxide layer. This has been demonstrated by Czernohorsky et al., where a modified MBE growth process was developed in which the chemical potential of oxygen was optimized with respect to the electrical properties by introducing additional nonactivated molecular oxygen during growth to keep the partial pressure in the range of 10^{-7} mbar.[37] This was found to result in a sharp interface between Gd_2O_3 and Si (Fig. 9), free from any silicide inclusions as well as silicate or silicon oxide. Therefore, such layers are ideal candidates for investigating the manifestation of charge defects and their influence on the dielectric properties of epitaxial Ln_2O_3s.

Preliminary investigation of electrical properties of epitaxial layers grown under optimized conditions exhibited very promising characteristics, such as low capacitive equivalent thickness and low leakage current density (CET < 1 nm, $J \approx 10^{-1}$ A/cm^2). Gottlob et al. reported CET ~0.86 nm and a leakage current density of ~0.5 A. cm^{-2} at 1 V gate bias for MOS stacks consisting of ultra-thin Gd_2O_3 layers with CMOS-compatible fully silicided nickel-silicide (FUSI-NiSi) metal gate electrodes yields.[38] The CET trend observed for the MOS structures with Gd_2O_3 gate dielectric and FUSI-NiSi electrode combination met all ITRS targets for oxide thickness as well as leakage current values for high performance (HP), low operating power (LOP), and low standby power (LSTP) applications (Fig. 10). The reported CET values (without quantum–mechanical corrections) represent an upper limit of the achieved effective oxide thickness (EOT). Assuming a quantum–mechanical correction of 0.3 nm to obtain EOT values shifts the trend line to an even more desirable region of specifications.[6] These results indicated that NiSi/Gd_2O_3 gate stacks with optimized oxide/Si interface properties could be quite promising candidates for scaling efforts to the limit of CMOS. However, despite the outstanding structural qualities, compatibility with CMOS process techniques including metal gate incorporation and encouraging electrical properties the epitaxial Gd_2O_3 layers (or for that matter other insulating Ln_2O_3s) suffer from several performance related issues which are required to be addressed prior to real device integration. For example, the MOS structure exhibiting EOT ~0.86 nm shows strong hysteresis (~120 mV) in the capacitance–voltage (*C–V*) profile when the gate bias between forward and backward sweeps at 500 kHz. The hysteretic feature of the *C–V* profile indicates presence of charge defects inside

Downloaded from https://www.cambridge.org/core. Technische Informationsbibliothek, on 05 Feb 2018 at 14:17:50, subject to the Cambridge Core terms of use, available at https://www.cambridge.org/core/terms. https://doi.org/10.1557/jmr.2017.22

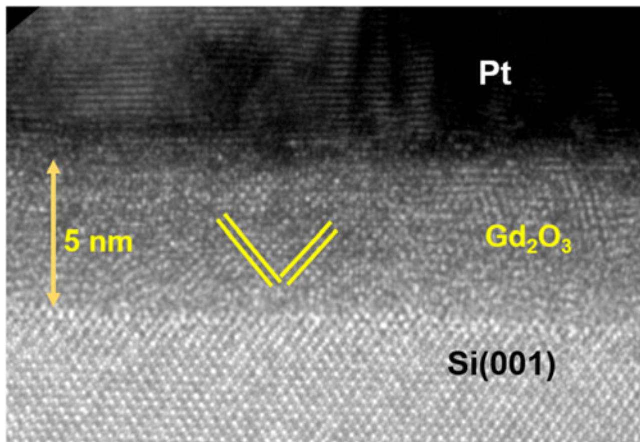

FIG. 9. High-resolution cross-sectional TEM micrograph of a $Pt/Gd_2O_3/Si(001)$ stack. The oxide layer is grown at under a molecular oxygen partial pressure of 5×10^{-7} mbar. Sharp interface without any amorphous interfacial layer is visible.

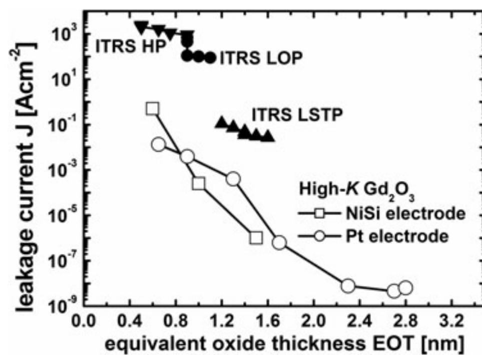

FIG. 10. Leakage currents versus EOT for ITRS (edition 2005) HP, LOP, LSTP target values, and data epitaxial Gd_2O_3 layers with different electrodes.

the oxide layer and/or oxide/Si interface. Gottlob et al. attributed this to oxide traps ($Q_{ot} = 3 \times 10^{12}$ cm^{-2}).[38] Such hysteresis represents flat band voltage (V_{FB}) instability of the dielectric layer which leads to unstable threshold voltage in transistors. This clearly establishes that excellent structural quality of the alternative high-*k* dielectric does not guarantee satisfactory device performance due to the presence of electrically active charge defects.

A. Charge defects in epitaxial lanthanide oxides

In MOS structures there can be different types of charge defects that can degrade their electrical performance, such as oxide fixed charge (Q_f), interface traps (Q_{it}), and mobile oxide charges (Q_m). In addition to unstable threshold voltage and instability of transistor operating characteristics, charge defects scatters carriers in the channel and lowers the carrier mobility. Further, defects cause unreliability; which is the starting point for electrical failure and breakdown of the oxide. SiO_2, which is an almost ideal insulating oxide, has very low defect density. The low co-ordination number and high heat of formation of covalent SiO_2, that allow it to remain amorphous at typical CMOS processing temperature, helps to minimize the defect density via localized bonding rearrangement. Further, the defects at the Si/SiO_2 interface related to Si dangling bonds can be removed by rearranging the bonding network at the interface. Compared to SiO_2, high-*k* metal oxides normally contain more defects. The bonding in high-*k* metal oxides is highly ionic with higher coordination number which make them poor glass formers.[16] Therefore, it is difficult to rearrange the bonds in the metal oxides for defect passivation. Since the charge defects in high-*k* dielectrics are undesirable for device applications for obvious reasons, much of the present-day engineering of these oxides consists of pragmatic strategies of trying to reduce defect densities by processing control and annealing. In this section we discuss about the nature of different charge defects existing in epitaxial LnOs and at the Ln_2O_3/Si interface and their effective passivation to improve the dielectric performance.

Let us start with the issues related to the dielectric properties of as-grown epitaxial Gd_2O_3 layers. The as-grown single crystalline Gd_2O_3 thin films on Si usually suffer from strong flatband voltage (V_{FB}) instability and are not process robust. This could be due to incomplete passivation of intrinsic dangling bonds induced by the existing binding mismatch at the Gd_2O_3/Si interface. When a Gd_2O_3 layer is deposited on clean Si surface; inevitably, the layer always consists of some defects pertaining to the Si dangling bonds at the interface and also due to the very different chemical nature of Si substrate (covalent) and oxide (highly ionic). Despite the oxide being grown epitaxially on Si substrate, not all Si surface atoms would have an opportunity to bond with overgrown epi-Gd_2O_3 layer's atoms. Such defects remain unsaturated due to the difference in the lattice parameters and space groups of the oxide and Si substrate.[34]

For example, MOS structures consisting of epitaxial Gd_2O_3 grown on clean Si substrates with atomically sharp interface, exhibit a large shift in the flat band voltage toward negative gate bias direction during multiple *C–V* sweeping (Fig. 11), which infers to a large number of intrinsic/extrinsic defects present at the interface.[39] Such instability occurs due to the accumulation of mostly positive fixed charges at the Gd_2O_3/Si interface created during *C–V* sweeping,[39,40] which could significantly degrade the electrical performance of any device.[41,42] Laha et al. reported Q_f ~9.5×10^{12} cm^{-2} for epitaxial Gd_2O_3 on Si which is only two orders of magnitude lower than the atomic density of dangling bonds on

Downloaded from https://www.cambridge.org/core. Technische Informationsbibliothek, on 05 Jul 2018 at 11:17:20, subject to the Cambridge Core terms of use, available at https://www.cambridge.org/core/terms. https://doi.org/10.1557/jmr.2017.22

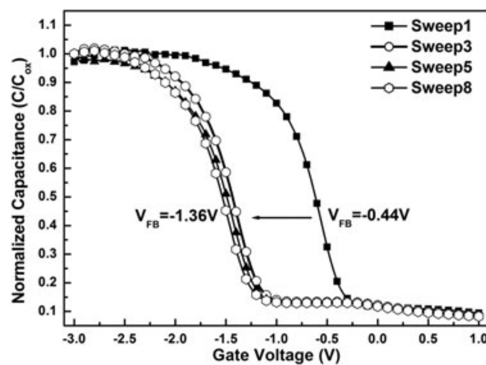

FIG. 11. *C–V* characteristics of single crystalline Gd_2O_3 on Si(100) substrate.

a nonreconstructed Si(001) surface. This implies that approximately 1% of Si surface bonds remain unsaturated even after oxide growth onto it.[40] Each Si surface atom possessing a dangling bond usually seeks an additional electron to become electrically neutral. They tend to capture the required electrons from the oxide layer near the interface, thereby creating large number electron vacancies, i.e., positive charges, which results in a large shift of the flat band voltage.

In addition to the shift in the V_{FB} under applied bias, MOS structures involving epitaxial Gd_2O_3 layers on Si also suffer from significant *C–V* hysteresis when the gate bias is cycled from accumulation to the inversion region and back. This hysteretic nature of the *C–V* characteristic is related to some sort of recharging process inside the dielectric. The origin of the observed hysteresis may not be unambiguously associated with some definite process. Nazarov et al. suggested that the *C–V* hysteresis in epitaxial Gd_2O_3/Si system could be attributed to both trapping of the holes inside the dielectric and recharging the electrons near-surface traps.[43] One of the major sources of charge trapping in the metal oxides is the omnipresent oxygen vacancies (V_Os) inside the layer, which give rise to defect states inside the band gap of the metal oxides. V_Os have been identified as critical trapping centers in diverse high-*k* metal oxides, such as HfO_2, ZrO_2, $LaAlO_3$ etc.[44,45] Further, in ionic metal oxides V_Os redistribution can also occur under sufficiently high electric field,[46,47] which can act as potential source of Q_m, thereby contributing at least partially to the observed *C–V* hysteresis. Czernohorsky et al. demonstrated that the hysteretic *C–V* characteristics of Gd_2O_3/Si heterostructures varies with P_{O_2} up to a certain limit, which clearly establishes the definitive role of V_Os on the hysteretic V_{FB} instability of epitaxial Gd_2O_3 layers.[37] It is obvious that such charge defects, which degrade the dielectric properties of epitaxial Ln_2O_3s, need to be minimized to improve their electrical performance prior to their integration into microelectronic devices.

V. PASSIVATION OF THE CHARGE DEFECTS IN EPITAXIAL LANTHANIDE OXIDES

In semiconductor industry one of the most commonly practiced method for passivation of charge defects in MOS structures is a thermal anneal in forming gas ambience. As a first measure for passivation of interface defect states in epitaxial Ln_2O_3s/Si heterostructures Sun et al. investigated forming gas anneal for the Gd_2O_3/Si system and found an influence of metal electrode.[39] For example, a post MOS fabrication anneal was found to be effective in case of tungsten electrode, whereas annealing prior to the electrode deposition was found necessary for Pt electrodes. Annealing epitaxial Gd_2O_3/Si system in forming gas environment at around 450 °C has been reported to reduce the Q_fs which stabilizes the V_{FB}. However, this approach is not only very specific to the electrode type, but is not effective for complete elimination of Q_fs in the epitaxial Ln_2O_3s. A negative shift in the flat band voltage (~ -0.44 V) for Pt/Gd_2O_3/Si stack has been reported even after the forming gas anneal of the MOS structures fabricated on p-type Si. The negative flat band voltage results from $Q_f \approx 2.3 \times 10^{12}/cm^2$, which is estimated using the relation: $Q_f = C_{ox}(V_{FB} - \Phi_{ms})$, where C_{ox} is the oxide layer capacitance and Φ_{ms} is the metal work function. Additionally, Pt/Gd_2O_3/Si stacks possess a large density of trapped interface charges ($D_{it} \sim 7.63$–8.8×10^{11} cm^{-2}).[39] These findings clearly indicate that forming gas anneal is an inadequate method to provide acceptable electrical properties for epitaxial Ln_2O_3s. Moreover, post deposition anneal also involves the risk of creating uncontrolled interfacial layer, exhibiting smaller dielectric constant as well as results in loss of epitaxy. As an alternative to forming gas anneal, Laha et al. demonstrated that the electrical properties of Gd_2O_3/Si structures can be improved significantly by interface engineering that involves atomic control growth of a silicate-like interfacial structure prior to the Gd_2O_3 layer.[48] However, controlling the interface composition is quite tedious and it involves multiple steps for substrate's surface preparation which renders the method less preferred for device fabrication. Another viable alternative surface preparation approach could be the passivation of Si dangling bond states by suitable chemisorbed species prior to the oxide layer growth. For examples, it has been widely reported that an ultrathin Si layer is very effective to passivate Ge surfaces for deep sub-micron p- and n-field effect transistor (FET) application,[49–51] whereas similar investigation for the effect of Ge on Si based devices is not commonplace. But it can be expected that deposition of Ge onto Si surface has also significant impact on the surface charge states of Si. It is known that a submonolayer (ML) Ge deposited onto a Si(111) surface leads to a charge transfer from the center Si adatoms

Downloaded from https://www.cambridge.org/core. Technische Informationsbibliothek, on 05 Feb 2018 at 14:17:50, subject to the Cambridge Core terms of use, available at https://www.cambridge.org/core/terms. https://doi.org/10.1557/jmr.2017.22

near the faulted half unit cell (FHUC) of a Si(111) (7 × 7) unit cell to the nearby Ge atoms, which makes the dangling bond states of Si adatoms empty.[52] In principle this effect might have significant impact on subsequent properties of devices built on such Si surfaces. Laha et al. investigated the influence of chemisorbed Ge layer on the growth and dielectric properties of epitaxial Gd_2O_3 layers on Si.[40] In this approach different amount of Ge (0.15–3 ML) was deposited by e-beam evaporation on clean Si surfaces prior to the Gd_2O_3 layer growth. The *in situ* RHEED patterns of the Gd_2O_3 layers grown on such Ge-covered Si surfaces (Fig. 12) are very similar to what has been observed for the layers grown pristine Si surfaces.[53] This demonstrates that despite the large lattice mismatch between Si and Ge, few MLs of Ge pre-coverage (Φ_{Ge}) does not have any impact on the growth and structure of the Gd_2O_3 layer for Φ_{Ge} at least up to 2 ML. Figure 13 compares the *C*–*V* characteristics of Gd_2O_3 layers grown on pristine Si surface and on a Ge pre-covered Si surface. A strong V_{FB} instability corresponding to Q_f $\sim 9.5 \times 10^{12}$ cm^{-2} was observed in case of Gd_2O_3 grown on Si surface without Ge passivation, whereas for Si passivated with 1.5 ML Ge a much stable and ideal-like *C*–*V* characteristics was obtained. A systematic increase in Φ_{Ge} leads to a monotonic increase in V_{FB} up to a maximum value of 0.3 V for 1.5 ML of Ge coverage [Fig. 14 (a)]. Further increase of Ge coverage was reported to result in nonuniformity in *C*–*V* measurements across the wafer.[40] The estimated V_{FB} in this case (+0.3 V) indicates negligible amount Q_f present at the interface. This improvement in the dielectric properties of the Gd_2O_3 layers was found to be independent of the Si surface orientation. It was also found that Ge pre-coverage on Si surface improves the density of interface traps significantly [Fig. 14 (b)], which also led to significant reduction in the hysteresis of the *C*–*V* characteristic.[40] These results clearly indicate that Ge deposition prior to the oxide layer growth significantly influence the electronic properties of Si surfaces and, consequently, the oxide/Si interface. To understand the influence of Ge on the surface electronic properties, Laha et al. also investigated the Si(111) surface states with different Φ_{Ge} using UPS. Figure 15 displays the photoemission spectra of Si(111) surfaces with different Φ_{Ge}. For pristine Si(111)-(7 × 7) surfaces ($\Phi_{Ge} \sim 0$), the well-known signals related to the adatom state (S_1), the rest atom state (S_2), and the back-bond state (S_3), are visible at energies close to the Fermi level (E_F).[54,55] In contrast, the spectra from the Ge covered Si(111) surface exhibits only two surface states measured under the same condition, one (B_1) about 0.38 eV and the other about 1.70 eV (B_3) below the Fermi level. The first peak corresponds to the adatom state of clean Si(111)-(7 × 7) surface, whereas the energetic position of the second peak (B_3) is located in between the S_2 and S_3 states of the clean Si surface. These results are in accordance to the earlier report by Carlisle et al.,[56] where it was found that with increasing Φ_{Ge} (>0.3 ML), rest-atom and back-bond surface states merge into one broad feature located approximately halfway between them.[57] Such changes in the surface states indicate significant change in the atomic arrangement of the Si surface due to Ge deposition. For example, in case of Si(111) the chemisorbed Ge atoms randomly occupy the Si adatom positions at the very early stage ($\Phi_{Ge} < 0.1$ ML). However, with increasing coverage they preferentially occupy the corner adatoms' position in the FHUC of Si (111)(7 × 7) surface structure.[58,59] At higher coverage ($\Phi_{Ge} > 0.5$ ML), Ge atoms form nanoparticles on FHUC side consisting of approximately eight atoms.[52,60] In the presence of Ge nanoparticles, the Si center adatoms transfer charges to the nearby Ge atoms and thereby dangling bond states of such adatoms become partly empty.[52] Such charge transfer from Si to Ge occurs due to the difference in electronegativity and the compressive strain in Ge layer. Consequently, dipoles form at the Si/Ge interface with an excess of 0.1 electrons on the Ge side.[61] Similar behavior has also been reported

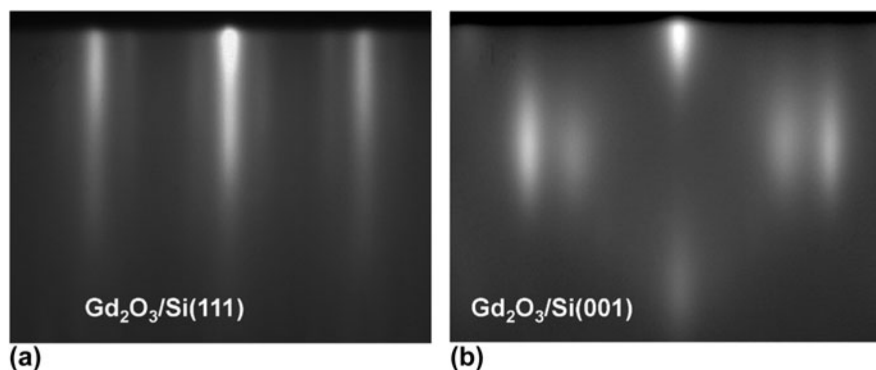

FIG. 12. RHEED patterns of epitaxial Gd_2O_3 on (a) Si(111) and (b) Si(001) substrates. 2 ML Ge was deposited on Si surface prior to the oxide layer growth. (Reprinted from Ref. 40 with permission of AIP publishing).

Downloaded from https://www.cambridge.org/core. Technische Informationsbibliothek, on 05 Jan 2018 at 14:17:20, subject to the Cambridge Core terms of use, available at https://www.cambridge.org/core/terms. https://doi.org/10.1557/jmr.2017.22

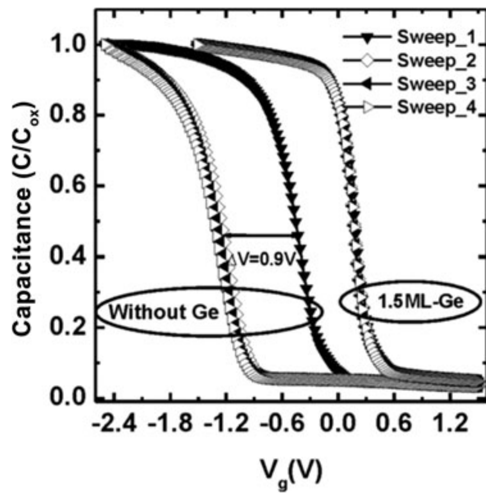

FIG. 13. $C–V$ characteristics of Pt/Gd_2O_3/Si(001) MOS capacitors depicting the effect of 1.5 ML Ge coverage on Si(001) substrates. The capacitors fabricated on Ge passivated Si surface exhibit improved $C–V$ behavior. (Reprinted from Ref. 40 with permission of AIP publishing).

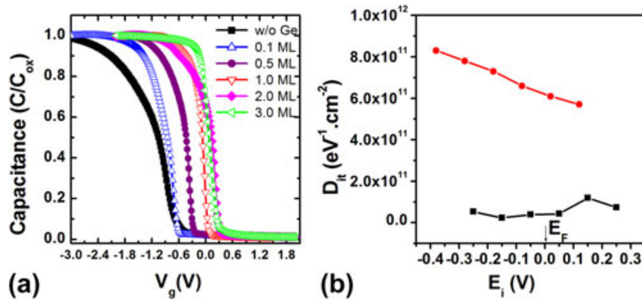

FIG. 14. (a) The $C–V$ characteristics of Pt/Gd_2O_3/Si(111) MOS capacitors as a function of Ge coverage. The flat band voltage increases monotonically with increasing Ge coverage up to ~1.5 ML. (b) Density of interface traps for Pt/Gd_2O_3/Si capacitors fabricated on clean and Ge passivated Si(111) wafers, exhibiting significant improvement on D_{it} values.

by various other groups for the Si(001) surfaces,[62,63] despite their different microstructure.[64]

Therefore, the observed reduction in fixed oxide charge density in the Gd_2O_3/Si interface can mainly be attributed to the charge transfer from Si dangling bonds toward Ge. In case of Gd_2O_3 growth on Si without pre-deposited Ge the remaining dangling bonds in the oxide/Si interface attempt to capture additional electrons from oxide regions close to the interface to become electrically neutral. Thereby, large number electron vacancies will be created, i.e., positive charges, which results in a large shift of V_{FB}. In contrast, when epitaxial Gd_2O_3 is grown on a Ge passivated surface, the contribution of the adatom dangling bond states significantly decreases. Moreover, due to the higher electron density at the top Ge layer owing to dipole formation, it is very unlikely that the electrons from the oxide interface

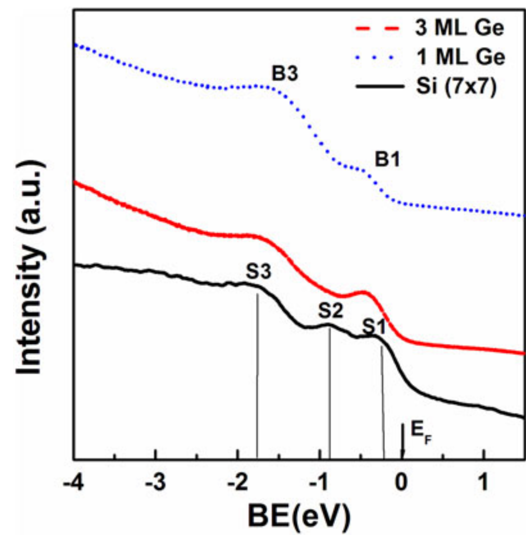

FIG. 15. UPS spectra from clean Si(111) (7 × 7) surfaces with different Ge coverage, obtained at a photon energy of 21.2 eV. The spectra were recorded along ⟨11−2⟩ azimuth at an emission angle of 5° with respect to surface normal.

would be captured by the underlying substrates, which leads to much more stable interface.

A reduction in fixed oxide charge density in the Gd_2O_3/Si interface and resultant improvement in the V_{FB} stability of epitaxial Gd_2O_3/Si structures was observed also for oxide layers grown on Si covered by submonolayer carbon,[65] indicating a similar charge transfer effect. Moreover, it was established that V_{FB} can be tailored by tuning the concentration of the chemisorbed species which can provide additional flexibility for device operation.[40,65,66] These observations establish the proof of principle about defect minimization at the oxide/Si interface by Si dangling bond passivation via charge transfer from Si adatoms to isovalent chemisorbed species with higher electronegativity.

Although surface passivation of Si by isoelectronic elements (Ge or C) prior to the oxide layer growth is a simple and effective way to reduce the fixed oxide charge and trap densities at the epitaxial Gd_2O_3/Si interface, this cannot completely eliminate the hysteretic $C–V$ characteristics of the MOS structures. As discussed in the previous section, in addition to charging effect, the hysteresis in $C–V$ could be partially related to the mobile charge defects inside the oxide layer owing to V_Os. Earlier we observed that with an increase in oxygen chemical potential during the oxide layer growth by an increase in P_{O_2} from 1×10^7 mbar to 5×10^7 mbar, the hysteresis also reduces significantly (Fig. 16).[37] However, a monotonic increase in P_{O_2} does not ensure complete elimination of the V_Os in the oxide layers.[37] Moreover, the magnitude of the flatband voltage change from voltage cycling ($\Delta V_{FB} > 40$ mV) was still beyond the acceptable value ($\Delta V_{FB} < 20$ mV) for stable transistor operation.[12]

Downloaded from https://www.cambridge.org/core. Technische Informationsbibliothek, on 05 Feb 2018 at 14:17:50, subject to the Cambridge Core terms of use, available at https://www.cambridge.org/core/terms. https://doi.org/10.1557/jmr.2017.22

Therefore, to minimize the V_Os related defects various post growth processing techniques have also been attempted to compensate those defects in different ionic oxides. However, as already mentioned above with regard to the thermal anneal in forming gas ambience, post growth processing which often involves annealing at high temperature sometimes degrades the overall electrical properties due to the formation of interfacial layers with inferior dielectric constants.[67,68] Alternatively, incorporation of dopants has been reported to be a viable route to improve the electrical properties of different oxides by reducing the influence of V_Os. For example, first principle calculations suggested that nitrogen (N) incorporation in Hf based dielectrics can reduce the leakage current conduction by effectively deactivating V_Os related gap states.[69] Substantial improvement of electrical properties has also been reported for HfO_2 thin films doped with fluorine, nitrogen, or lanthanum.[70–72]

To explore the possible influence of dopants on the electrical properties of epitaxial Ln_2O_3s, we investigated the influence of nitrogen incorporation on the dielectric properties of epitaxial Gd_2O_3 layers. Nitridation of the layers was achieved by using nonactivated molecular N_2O as process gas instead of O_2 during growth. The incorporation of nitrogen into the oxide layers was checked by secondary ion mass spectroscopy (SIMS). The formation of Gd–N bonds in the Gd_2O_3:N layers was confirmed by *in situ* XPS measurements from the chemical shift of the Gd 4*d* peaks toward lower binding energy compared to pure Gd_2O_3 layers.[73] However, a quantitative estimation of the N incorporated into the Gd_2O_3 layers by this approach is yet to be achieved. Layers with different amount of N were grown by maintaining different partial pressure of N_2O (P_{N_2O}) during deposition. All Gd_2O_3:N samples grown with different P_{N_2O} exhibited similar uniform distribution of N concentration across the oxide layer. Figure 17 displays the SIMS profile of a representative Gd_2O_3:N sample which confirms the presence of N inside the oxide layer.

Further, to understand the impact of N incorporation on the growth of Gd_2O_3 and the electrical properties of MOS stacks with epitaxial Gd_2O_3:N on Si, these layers were compared with control Gd_2O_3 layers grown with similar partial pressure of molecular oxygen.[73,74] The streaky RHEED patterns [Fig. 18(a)] exhibited by the Gd_2O_3:N layer surface indicate the same two-dimensional growth on Si(111) as observed for undoped oxide. Figure 18(b) compares the X-ray diffraction patterns of two Gd_2O_3:N layers grown at different N_2O partial pressures with a control Gd_2O_3 layer in the θ–2θ geometry. The shoulder observed at 2θ ~28.9° beside the Si(111) peak corresponds to the (111) oriented epitaxial Gd_2O_3 with cubic bixbyite type of structure.

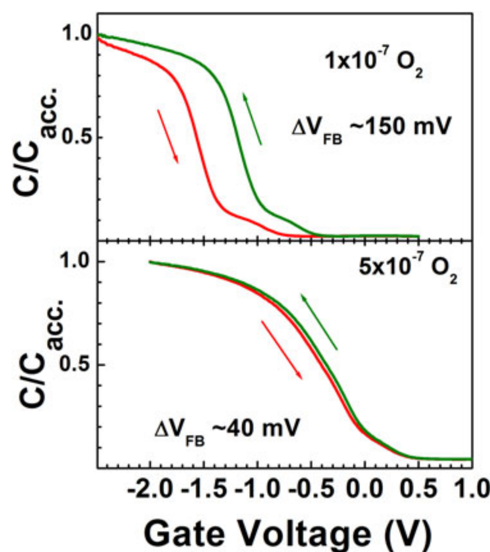

FIG. 16. *C–V* characteristics of two epitaxial Gd_2O_3 layers on Si(001) substrates grown at different oxygen partial pressures.

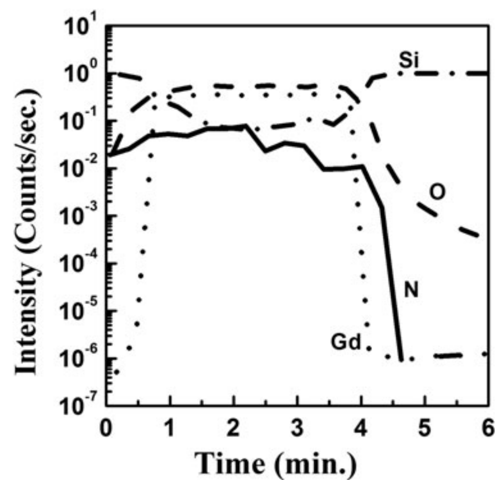

FIG. 17. SIMS depth profile of Gd, O, N and Si elements of a representative Gd_2O_3:N sample as function of etching time.

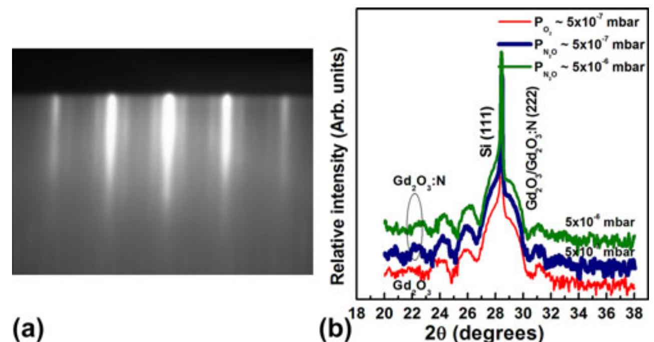

FIG. 18. (a) RHEED pattern along the ⟨110⟩ azimuth of a representative Gd_2O_3:N layer (P_{N_2O} ~5×10^{-7} mbar) and (b) X-ray diffraction patterns in the θ–2θ geometry of a control Gd_2O_3 layer and two representative Gd_2O_3:N layers.

Downloaded from https://www.cambridge.org/core. Technische Informationsbibliothek, on 05 Feb 2018 at 14:17:20, subject to the Cambridge Core terms of use, available at https://www.cambridge.org/core/terms. https://doi.org/10.1557/jmr.2017.22

These results indicate that usage of N_2O as a process gas incorporates N into the Gd_2O_3 layers only at a doping level and it does not affect the growth and structure of the layers.

However, a dramatic change in the dielectric properties of the epitaxial Gd_2O_3 layers was observed due to N incorporation. Figure 19 compares the *C–V* characteristics of a Gd_2O_3 and a Gd_2O_3:N sample grown under lower partial pressure of the process gases ($\sim 2 \times 10^{-7}$ mbar). The control sample prepared under reduced P_{O_2} [Fig. 19(a)] exhibits a strong hysteresis in the *C–V* behavior inferring that there exist a large number of mobile oxide charges inside the oxide layer. A density of $Q_m \sim 2 \times 10^{12}$ cm^{-2} was estimated from the hysteretic shift of the V_{FB} ($\sim$140 mV) assuming only Q_m contribution to the *C–V* hysteresis. In contrary, in case of N doping [Fig. 19(b)] hysteresis in *C–V* was nearly vanished with $\Delta V_{FB} < 10$ mV corresponding to a $Q_m < 1 \times 10^{11}$ cm^{-2}. This clearly demonstrates that nitridation of Gd_2O_3 even at a low level (lower P_{N_2O}) already results in a nearly ideal dielectric behavior, likely due to an effective compensation of mobile oxide charges.

The influence of doping by other species has also been investigated by introducing carbon into Gd_2O_3. C incorporation in different high-*k* oxides was reported to improve their dielectric properties.[75,76] In our investigation, incorporation of C into the epitaxial Gd_2O_3 layers was found to result also in a significant improvement in the dielectric properties of MOS structures (i.e., minimize *C–V* hysteresis and lower leakage current density) for C concentration below 0.5%.[47,77] However, at higher concentration, C segregates to the oxide/Si interface during growth. That leads to polycrystallinity and degradation of the electrical properties due to the formation of additional defects,[47,66] which makes it less preferred choice for doping Gd_2O_3 compared to N.

In addition to their impact on the dielectric properties, the dopants can also have significant influence on the electronic structure of high-*k* oxides. For example, density functional calculations revealed that incorporation of N into high-*k* oxides leads to a reduction of their band gap and the VBO with Si which could result in degradation of the MOS electrical properties.[78] Therefore, to gain a holistic understanding, the impact of N incorporation into epitaxial Gd_2O_3 layers on its band structure and dc leakage properties were also investigated. The electronic structure of the oxide layers were probed using *in situ* XPS measurement. Valence band photoelectron spectra of the layers were used to estimate the impact of N doping on the VBO of Gd_2O_3 with Si, which was determined from the relation:

$$\Delta E_V = \left(E_{CL}^{Ox} - E_V^{Ox}\right) - \left(E_{CL}^{Si} - E_V^{Si}\right) - \Delta E_{CL} \quad , \qquad (1)$$

where $\left(E_{CL}^{Ox} - E_V^{Ox}\right)$ and $\left(E_{CL}^{Si} - E_V^{Si}\right)$ are the core level to valence band maximum (VBM) energy difference for bulk Gd_2O_3 or Gd_2O_3:N and Si, respectively, and ΔE_{CL} is the separation between a certain core level of the oxide (O 1*s*) and Si (Si 2*p*). The parameters for Si were measured from an identical bare Si wafer. The Si 2*p* peak position, measured under the presence of a thin oxide layers ($\sim$2 nm) at the Si surface, was found to be independent on the nature and the partial pressure of the processing gas (O_2 or N_2O) applied during the epitaxial layer growth, and, moreover, no notable difference in the oxide peak position was observed for samples with different thicknesses. Since the VBM for Si was nearly zero, the VBO between Gd_2O_3:N or Gd_2O_3 and Si could be directly determined from the position of the VBM of the oxide layers on Si. Figure 20 presents the VB photoelectron spectra of a control Gd_2O_3 sample and Gd_2O_3:N samples grown on Si at different P_{N_2O}. A value of 2.4 ± 0.2 eV was obtained for VBO for all control Gd_2O_3 samples grown at different P_{O_2}, which is in good agreement to an earlier report.[48] Doping of Gd_2O_3 with N leads to a reduction of the VBO with Si. Thereby, the VBO value of Gd_2O_3N was found to reduce progressively with increasing P_{N_2O} from 2.2 ± 0.2 eV

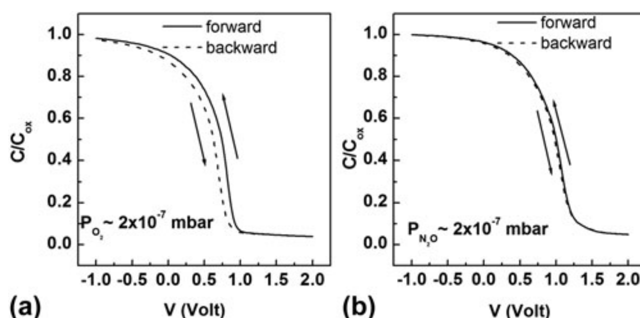

FIG. 19. Representative *C–V* hysteresis curves corresponding to (a) a control epitaxial Gd_2O_3 samples and (b) an epitaxial Gd_2O_3:N sample.

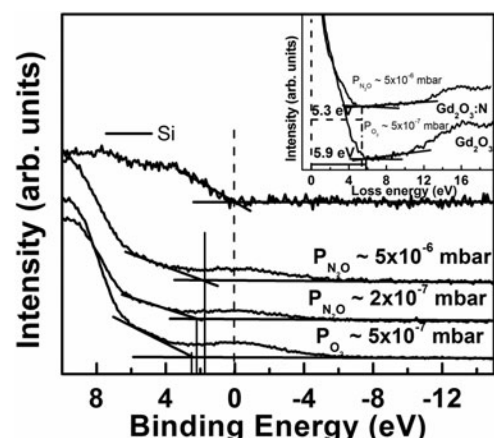

FIG. 20. Valence Band spectra for Si, a control Gd_2O_3 layer and two Gd_2O_3:N layers, (inset) O 1*s* energy loss spectra of a control Gd_2O_3 layer and a Gd_2O_3:N layer.

Downloaded from https://www.cambridge.org/core. Technische Informationsbibliothek, on 05 Feb 2018 at 14:17:50, subject to the Cambridge Core terms of use, available at https://www.cambridge.org/core/terms. https://doi.org/10.1557/jmr.2017.22

for P_{N_2O} ~2×10^{-7} mbar up to a value of 1.7 ± 0.2 eV at P_{N_2O} ~2×10^{-6} mbar. Further increase of P_{N_2O} did not influence the VBO under present experimental conditions, inferring saturation in the concentration of N incorporated into the Gd_2O_3 layer.

In further investigations, the band gaps of the Gd_2O_3:N and control Gd_2O_3 layers were estimated in XPS from the threshold energy of the plasmon energy loss spectrum observed at higher binding energy of the O 1*s* core level peak, as already demonstrated for other metal oxides.[26] As shown in the inset of Fig. 20, the extrapolation yields a band gap energy of 5.9 ± 0.2 eV for the control sample, which agrees very well to the previously reported values for epitaxial Gd_2O_3 layers on Si.[48] In contrast, the band gap of the Gd_2O_3:N layers was found to decrease from 5.7 ± 0.2 eV for a layer grown at P_{N_2O} ~2×10^{-7} mbar to 5.2 ± 0.2 eV for a layer grown at P_{N_2O} ~2×10^{-6} mbar.

The band gap narrowing and reduction in VBO of epi-Gd_2O_3:N with Si can be understood by considering the nature of the VB structure of the binary Ln sesquioxides. In case of the Ln sesquioxides the valence band maximum is formed mainly by the O 2*p* states.[79] In case of substitutional N incorporation in different lanthanide and transition metal oxides (e.g., La_2O_3, HfO_2), their upper VB levels are shared between both O 2*p* and N 2*p* states.[78] The energy level of the N 2*p* states lie above the O 2*p* states, which leads to a shift of the VBM toward higher energy, thereby reducing the VB offset of the N doped oxide layer with Si. The same is valid for Gd_2O_3, the increase of N content in the Gd_2O_3 layers causes the VBM to possess increasing N 2*p* character, which leads to the gradual reduction of the band gap and VBO with Si, until saturation. The conduction band offsets (CBOs) estimated for the Gd_2O_3/Si structures considering the differences in the VBO, the energy gap of the Si substrate (~1.12 eV) and the measured band gap of the oxide were found to be nearly identical (2.4 ± 0.2 eV) for all the Gd_2O_3 and Gd_2O_3:N samples; indicating that the CB of the oxide layers remains nearly unaffected by N doping, that agrees well with *ab initio* calculations reported for related oxides.[78]

The reduction in the VBO with Si due to N incorporation can be expected to degrade the insulating properties of the Gd_2O_3:N layer owing to lower hole barrier. However, as demonstrated for a representative set of samples in Fig. 21(a), the room temperature dc leakage measurements revealed that at applied electric fields below 4 MV/cm all the Gd_2O_3:N samples grown under different P_{N_2O} exhibit lower leakage current densities compared to the control Gd_2O_3 samples grown under similar P_{O_2} indicating their superior insulating properties. For example, at 1 V (V_{FB} −1 V), the leakage current densities of the Gd_2O_3:N layers were found to be about

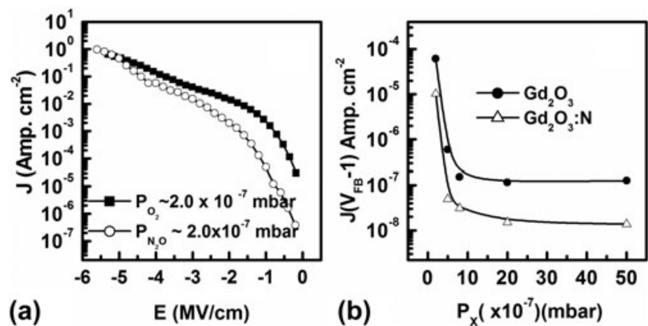

FIG. 21. (a) Room temperature dc leakage current densities of a representative Gd_2O_3 and a Gd_2O_3:N layer. (b) dc leakage current densities measured at 1 V for different Gd_2O_3 and Gd_2O_3:N samples as functions of ambient gas partial pressure (P_X) during growth. X denotes O_2 in case Gd_2O_3 and N_2O in case of Gd_2O_3:N layers. The lines are to guide the eyes.

one order of magnitude lower compared to the control samples [Fig. 21 (b)].

The superior insulating properties of the Gd_2O_3:N layers can be explained by considering the influence of N on the electrically active defects in Gd_2O_3, especially on V_Os, which are the most dominating electrically active defect in complex oxides grown at higher temperatures.[80,81] Experimental investigations and *ab initio* calculations revealed that V_Os induce electron conduction paths in complex oxides which give rise to enhanced leakage current densities.[82–85] The same can be suggested for epitaxial Ln_2O_3s. In case of ionic oxides, this occurs via V_Os induced energy states within the band gap, which are occupied by two electrons for the neutral vacancy (V^0_O) and are strongly localized on the orbitals of the adjacent metal ions.[66,80,83] Moreover, migration of V_Os under sufficiently large electric field can also give rise to an increase in the leakage current densities in complex oxides.[86–88] Lowering of the leakage current densities by incorporation of N into Gd_2O_3 layers can be understood in much the same way as the elimination of the hysteresis effect in *C–V* measurements of nitrogen-doped Gd_2O_3 by considering the specific role of N in compensating the adverse effects the V_Os related defects. In analogy to the effect of N incorporation in various other ionic oxides, this can only happen either due to the formation of N–V_Os complexes and/or substitution of the V_Os by N atoms in the Gd_2O_3:N. First principle calculations of N incorporation in different oxides suggested that in a minimum free energy configuration two N atoms occupy the nearest neighbor O sites to V_Os.[69,89] In this arrangement each N atom extracts one electron from the neutral V_O sites to form a closed shell electronic configuration. Consequently, neutral V_Os transform into positively charged V_O^{2+} forming electric dipoles, which effectively elevates the energy of the V_O related gap states above the conduction band of these oxides. In this way the dc leakage conduction is reduced.[69,80]

Downloaded from https://www.cambridge.org/core. Technische Informationsbibliothek, on 05 Feb 2018 at 11:41:20, subject to the Cambridge Core terms of use, available at https://www.cambridge.org/core/terms. https://doi.org/10.1557/jmr.2017.22

In analogy, the observed improvement in the dielectric properties of the Gd_2O_3:N layers could be attributed to a similar mechanism when N atoms combine favourably to the V_O sites in Gd_2O_3 and modify their charge states. Moreover, N atoms can also immobilize the V_Os which can in turn reduce the V_Os motion related leakage current conduction under an applied electric field.[69] The effect gets more pronounced with increasing N content in the Gd_2O_3:N layers grown at higher P_{N_2O}. Further, the electric field corresponding to dielectric breakdown was found to be in the range of 4.5–5 MV/cm for all the samples, which agrees to the thermochemical description of dielectric breakdown in high-*k* materials.[90,91] However, in case of the Gd_2O_3:N layers the breakdown field was found to reduce with increasing N content. Such reduction in the dielectric breakdown field could be attributed to a collective effect of the reduced VB offset and an enhanced local electric field in the Gd_2O_3 layer due to N incorporation.[90,91]

VI. SUMMARY AND OUTLOOK

We discussed different ways of growth optimization for improvement of dielectric properties of insulating Ln_2O_3 epitaxial grown on Si using molecular beam epitaxy. The growth optimization and discussion involves the density of charge defects inside the oxide layer as well as the oxide/Si interface, their impacts on the dielectric properties of oxide/Si heterostructures and different methods to passivate the charge defects. As a standard material we have considered epitaxial Gd_2O_3 layers to discuss the proof of principles. We demonstrated that the best vacuum condition achieved in the MBE chamber during oxide layer growth ($\sim 10^{-8}$ mbar) leads to silicide formation at the interface, which degrades the dielectric properties of the oxide layers. A controlled supply of molecular oxygen during the growth improves the interface quality significantly, however too high oxygen partial pressure leads to formation of lower permittivity interfacial layer and finally limits the achievable minimum effective oxide thickness. Partial pressure of oxygen in the range 10^{-7} mbar was found to be optimal to achieve epitaxial layers having atomic sharp interface to Si. Although such layers exhibit good dielectric properties in terms of the effective oxide thickness, as grown epitaxial Ln_2O_3s exhibit strong shift of the flatband voltage toward negative gate bias direction and also suffer from hysteretic flat band instability which render them unsuitable for transistor applications. In view of understanding the origin of flat band instability, we discussed the nature of fixed oxide charges in the epitaxial layers and their impact on the dielectric properties. The unsaturated dangling bond states in the oxide/Si interface were found to be responsible for the creation of positive charges inside the oxide layer, since they captures electrons form the oxide layer near to the interface. In addition to the fixed oxide charges, interface traps and mobile oxide charges originating from omnipresent oxygen vacancy related defect states also degrade the dielectric properties of the oxides. Consequently, these defects are required to be minimized prior to integrating these oxides into the Si technology for device application.

We have discussed different possible methods of defect passivation, such as annealing, doping and surface passivation by foreign atoms. Annealing the Ln_2O_3 layers in forming gas ambience, which is one of the most commonly used method for defect passivation in microelectronic materials, stands inadequate due to its sensitivity to the type of the metal gate used. As a viable alternative to this approach we have demonstrated that few monolayers of chemisorbed Ge or C on Si surface significantly improves the electrical properties of MOS structures with epitaxial Gd_2O_3 layers by passivation the Si dangling bond states. This happens due to the charge transfer from the dangling bonds of Si to the Ge or C atoms owing to the difference in their electronegativity. The passivation of the fixed oxide charges and interface traps stabilizes the flat band voltage and reduces hysteresis. Moreover, the flat band voltage can be tuned systematically by precisely controlling the amount of the chemisorbed species.

Incorporation of nitrogen into the oxide layers in a doping level was found to be a suitable way for passivation mobile oxide charges inside the layers, which results in vanishing flat band voltage hysteresis. Incorporation of N into the epitaxial Gd_2O_3 layer results in a band gap narrowing, which is related to the shift of valence band edge in Gd_2O_3:N layers toward higher energy due to their presumably increasing N 2*p* character in the valence band edge. Despite the declining VBOs with Si, the dc leakage current densities of epitaxial Gd_2O_3 layers is reduced significantly by N doping. These observations suggest that N incorporation in a doping level can improve the overall electrical properties of epitaxial Ln_2O_3s by passivation the detrimental effects of the electrically active V_Os related defect states. Therefore, it appears that suitably doped epitaxial Ln_2O_3 layers deposited on surface Si surfaces, which are passivized with chemisorbed Ge, can be ideal candidate materials for next generation high-*k* dielectric applications. However, it should be noted that the extent to which the band gap of Gd_2O_3:N and its band offsets with Si can be tuned by increasing the N doping concentration still remains unclear. Furthermore, the impact of oxide doping and oxide/Si modification by Ge predeposition in active devices, such as CMOS based FET, is not yet tested in practice.

ACKNOWLEDGMENT

This paper reviews research results we have been working on for the last 10 years at the Institute of

Downloaded from https://www.cambridge.org/core. Technische Informationsbibliothek, on 05 Feb 2018 at 14:17:50, subject to the Cambridge Core terms of use, available at https://www.cambridge.org/core/terms. https://doi.org/10.1557/jmr.2017.22

Electronic Materials and Devices, Leibniz University Hannover. We are grateful to all PhD students and scientist working with us on particular aspects of that challenging project. We also would like to thank all partners and friends in Germany and all over the world for intense collaboration and help. Finally, we acknowledge the support of various organisations, in particular DFG (Deutsche Forschungsgemeinschaft), BMBF (Bundesministerium für Forschung und Technologie), DAAD (Deutscher Akademischer Austauschdienst), Humboldt Foundation, and GIF (German-Israel Foundation for Scientific Research and Development).

REFERENCES

1. G.E. Moore: Cramming more components onto integrated circuits. *Electronics* **38**, 114ff (1965).
2. M.L. Green, E.P. Gusev, R. Degraeve, and E.L. Garfunkel: Ultrathin (<4 nm) SiO_2 and Si–O–N gate dielectric layers for silicon microelectronics: Understanding the processing, structure, and physical and electrical limits. *J. Appl. Phys.* **90**, 2057 (2001).
3. G. Pahionni: Defects in SiO_2 and related dielectrics: Science and Technology (Kluwer Academic Publishers, Dordrecht, 2000); p. 1.
4. H.J. Osten, M. Czernohorsky, R. Dargis, A. Laha, D. Kuehne, E. Bugiel, and A. Fissel: Integration of functional epitaxial oxides into silicon: From high-*k* application to nanostructures. *Microelectron. Eng.* **84**, 2222 (2007).
5. G. Timp, J. Bude, K.K. Bourdelle, J. Garno, A. Ghetti, H. Gossmann, M. Green, G. Forsyth, Y. Kim, R. Kleiman, F. Klemens, A. Kornblit, C. Lochstampfor, W. Mansfield, S. Moccio, T. Sorsch, D.M. Tennant, W. Timp, and R. Tung: The ballistic nano-transistor. *IEDM Tech. Dig.* **99**, 55 (1999).
6. The latest edition of the ITRS road map can be found at http:/www.itrs2.net.
7. Z.J. Ma, J.C. Chen, Z.H. Liu, J.T. Crick, Y.C. Cheng, C. Hu, and P.K. Ko: Suppression of boron penetration in P^+ polysilicon gate P-MOSFET's using low-temperature gate-oxide N_2O anneal. *IEEE Electron Device Lett.* **15**, 109 (1994).
8. M. Cao, P.V. Voorde, M. Cox, and W. Greene: Boron diffusion and penetration in ultrathin oxide with poly-Si gate. *IEEE Electron Device Lett.* **19**, 291 (1998).
9. J. Robertson: High dielectric constant gate oxides for metal oxide Si transistors. *Rep. Prog. Phys.* **69**, 327 (2006).
10. E.P. Gusev, H-C. Lu, E.L. Garfunkel, T. Gustafsson, and M.L. Green: Growth and characterization of ultrathin nitrided silicon oxide films. *IBM J. Res. Dev.* **43**, 265 (1999).
11. J.D. Plummer and P.B. Griffin: Material and process limits in silicon VLSI technology. *Proc. IEEE* **89**, 240 (2001).
12. G.D. Wilk, R.M. Wallace, and J.M. Anthony: High-*k* gate dielectrics: Current status and materials properties considerations. *Appl. Phys. Rev.* **89**, 5243 (2001).
13. K.J. Hubbard and D.G. Schlom: Thermodynamic stability of binary oxides in contact with silicon. *J. Mater. Res.* **11**, 2757 (1996).
14. K. Cho: First-principles modeling of high-*k* gate dielectric materials. *Comput. Mater. Sci.* **23**, 43 (2002).
15. J. Robertson: Band offsets of wide-band-gap oxides and implications for future electronic devices. *J. Vac. Sci. Technol., B: Microelectron. Nanometer Struct.* **18**, 1785 (2000).
16. J. Lucovsky: Transition from thermally grown gate dielectrics to deposited gate dielectrics for advanced silicon devices: A classification scheme based on bond ionicity. *J. Vac. Sci. Technol., A* **19**, 1553 (2001).
17. G.D. Wilk and R.M. Wallace: Electrical properties of hafnium silicate gate dielectrics deposited directly on silicon. *Appl. Phys. Lett.* **74**, 2854 (1999).
18. R.J. Potter, P.A. Marshall, P.R. Chalker, S. Taylor, A.C. Jones, T.C.Q. Noakes, and P. Bailey: Characterization of hafnium aluminate gate dielectrics deposited by liquid injection metal-organic chemical vapor deposition. *Appl. Phys. Lett.* **84**, 4119 (2004).
19. Z.M. Rittersma, E. Naburgh, T. Dao, A.H.C. Hendriks, W.F.A. Besling, E. Tois, E. Vainonen-Ahlgren, M. Tuominen, and S. Haukka: Physical and electrical properties of Zr-silicate dielectric layers deposited by atomic layer deposition. *Electrochem. Solid-State Lett.* **6**, F21 (2003).
20. P.D. Kirsch, C.S. Kang, J. Lozano, J.C. Lee, and J.G. Ekerdt: Electrical and spectroscopic comparison of HfO_2/Si interfaces on nitrided and unnitrided Si(100). *J. Appl. Phys.* **91**, 4353 (2002).
21. K. Mistry, C. Allen, C. Auth, B. Beattie, D. Bergstrom, M. Bost, M. Brazier, M. Buehler, A. Cappellani, R. Chau, C-H. Choi, G. Ding, K. Fischer, T. Ghani, R. Grover, W. Han, D. Hanken, M. Hattendorf, J. He, J. Hicks, R. Huessner, D. Ingerly, P. Jain, R. James, L. Jong, S. Joshi, C. Kenyon, K. Kuhn, K. Lee, H. Liu, J. Maiz, B. McIntyre, P. Moon, J. Neirynck, S. Pae, C. Parker, D. Parsons, C. Prasad, L. Pipes, M. Prince, P. Ranade, T. Reynolds, J. Sandford, L. Shifren, J. Sebastian, J. Seiple, D. Simon, S. Sivakumar, P. Smith, C. Thomas, T. Troeger, P. Vandervoorn, S. Williams, and K. Zawadzki: A 45 nm logic technology with high-k + metal gate transistors, strained silicon, 9 Cu interconnect layers, 193 nm dry patterning, and 100% Pb-free packaging. *Proc. Tech. Dig. Int. Electron Dev. Meeting*, **247** (2007).
22. H.J. Osten, A. Laha, M. Czernohorsky, E. Bugiel, R. Dargis, and A. Fissel: Introducing crystalline rare-earth oxides into Si technologies. *Phys. Status Solidi A* **205**, 695 (2008).
23. G.V. Samsonov: *The Oxide Handbook*, 2nd ed. (IFI/Plenum, New York, 1982).
24. J. Robertson and K. Xiong: Electronic structure and band offsets of lanthanide oxides. *Top. Appl. Phys.* **106**, 313 (2007).
25. M. Foëx and J.P. Traverse: Investigations about crystalline transformation in rare earths sesquioxides at high temperatures (in French). *Rev. Int. Hautes Temp. Refract.* **3**, 429 (1966).
26. H. Nohira, W. Tsai, W. Besling, E. Young, J. Petry, T. Conard, W. Vandervorst, S. De Gendt, M. Heyns, J. Maes, and M. Tuominen: Characterization of ALCVD-Al_2O_3 and ZrO_2 layer using X-ray photoelectron spectroscopy. *J. Non-Cryst. Solids* **303**, 83 (2002).
27. M. Badylevich, S. Shamuilia, V.V. Afanas'ev, A. Stesmans, A. Laha, H.J. Osten, and A. Fissel: Investigation of the electronic structure at interfaces of crystalline and amorphous Gd_2O_3 thin layers with silicon substrates of different orientations. *Appl. Phys. Lett.* **90**, 252101 (2007).
28. A. Roy Chaudhuri, A. Fissel, and H.J. Osten: Superior dielectric properties for template assisted grown (100) oriented Gd_2O_3 thin films on Si(100). *Appl. Phys. Lett.* **104**, 012906 (2014).
29. A. Fissel, Z. Elassar, O. Kirfel, E. Bugiel, M. Czernohorsky, and H.J. Osten: Interface formation during molecular beam epitaxial growth of neodymium oxide on silicon. *J. Appl. Phys.* **99**, 074105 (2006).
30. A. Fissel, H.J. Osten, and E. Bugiel: Towards understanding epitaxial growth of alternative high-KK dielectrics on Si(001): Application to praseodymium oxide. *J. Vac. Sci. Technol., B: Microelectron. Nanometer Struct.* **21**, 1765 (2003).
31. H.J. Osten, J.P. Liu, E. Bugiel, H.J. Mussig, and P. Zaumseil: Growth of crystalline praseodymium oxide on silicon. *J. Cryst. Growth* **235**, 229 (2002).

Downloaded from https://www.cambridge.org/core. Technische Informationsbibliothek, on 05 Feb 2018 at 14:17:50, subject to the Cambridge Core terms of use, available at https://www.cambridge.org/core/terms. https://doi.org/10.1557/jmr.2017.22

32. F.P. Netzer: Rare earth overlayers on silicon. *J. Phys.: Condens. Matter* **7**, 991 (1995).
33. D.P. Norton, C. Park, Y.E. Lee, and J.D. Budai: Strontium silicide termination and silicate epitaxy on (001). *J. Vac. Sci. Technol., B: Microelectron. Nanometer Struct.* **20**, 257 (2002).
34. A. Fissel, J. Dabrowski, and H.J. Osten: Photoemission and ab initio theoretical study of interface and film formation during epitaxial growth and annealing of praseodymium oxide on Si(001). *J. Appl. Phys.* **91**, 8986 (2002).
35. E. Bugiel, H.J. Osten, A. Fissel, O. Kirfel, and M. Czernohosky: TEM investigations of epitaxial high-*k* dielectrics on silicon. *Microscopy of Semiconducting Materials* **107**, 343 (2005).
36. D. Schmeißer, J. Dabrowski, and H.J. Müssig: Pr_2O_3/Si(001) interface reactions and stability. *Mater. Sci. Eng., B* **109**, 30 (2004).
37. M. Czernohorsky, E. Bugiel, H.J. Osten, A. Fissel, and O. Kirfel: Impact of oxygen supply during growth on the electrical properties of crystalline Gd_2O_3 thin films on Si(001). *Appl. Phys. Lett.* **88**, 152905 (2006).
38. H.D.B. Gottlob, T. Echtermeyer, M. Schmidt, T. Mollenhauer, J.K. Efavi, T. Wahlbrink, M.C. Lemme, M. Czernohorsky, E. Bugiel, A. Fissel, H.J. Osten, and H. Kurz: 0.86-nm CET gate stacks with epitaxial Gd_2O_3 high-*k* dielectrics and FUSI NiSi metal electrodes. *IEEE Electron Device Lett.* **27**, 814 (2006).
39. Q.Q. Sun, A. Laha, S.J. Ding, D.W. Zhang, H.J. Osten, and A. Fissel: Effective passivation of slow interface states at the interface of single crystalline Gd_2O_3 and Si(100). *Appl. Phys. Lett.* **92**, 152908 (2008).
40. A. Laha, A. Fissel, and H.J. Osten: Effect of Ge passivation on interfacial properties of crystalline Gd_2O_3 thin films grown on Si substrates. *Appl. Phys. Lett.* **96**, 072903 (2010).
41. G.S. Lujan, W. Magnus, L.A. Ragnarsson, S. Kubicek, S.D. Gendt, M. Heyns, and K.D. Meyer: Modelling mobility degradation due to remote Coulomb scattering from dielectric charges and its impact on MOS device performance. *Microelectron. Reliab.* **45**, 794 (2005).
42. M. Casse, L. Thevenod, B. Guillaumot, L. Tosti, F. Martin, J. Mitard, O. Weber, F. Andrieu, T. Ernst, G. Reimbold, T. Billon, M. Mouis, and F. Boulanger: Carrier transport in HfO_2/metal gate MOSFETs: Physical insight into critical parameters. *IEEE Trans. Electron Devices* **53**, 759 (2006).
43. A.N. Nazarov, Y.V. Gomeniuk, Y.Y. Gomeniuk, H.D.B. Gottlob, M. Schmidt, M.C. Lemme, M. Czernohorsky, and H.J. Osten: Charge trapping in ultrathin Gd_2O_3 high-*k* dielectric. *Microelectron. Eng.* **84**, 1968 (2007).
44. K. Xiong, J. Robertson, M. Gibson, and S.J. Clark: Defect energy levels in HfO_2 high-dielectric-constant gate oxide. *Appl. Phys. Lett.* **87**, 183505 (2005).
45. K. Xiong, J. Robertson, and S.J. Clark: Defect states in the high-dielectric-constant gate oxide $LaAlO_3$. *Appl. Phys. Lett.* **89**, 022907 (2006).
46. G. Holzlechner, D. Kastner, C. Slouka, H. Hutter, and J. Feig: Oxygen vacancy redistribution in $PbZr_xTi_{1-x}O_3$ (PZT) under the influence of an electric field. *Solid State Ionics* **262**, 625 (2014).
47. A. Laha, B. Ai, P.R.P. Babu, A. Fissel, and H.J. Osten: Impact of carbon incorporation into epitaxial Gd_2O_3 thin films on silicon: An experimental study on electrical properties. *Appl. Phys. Lett.* **99**, 152902 (2011).
48. A. Laha, H.J. Osten, and A. Fissel: Influence of interface layer composition on the electrical properties of epitaxial Gd_2O_3 thin films for high-*K* application. *Appl. Phys. Lett.* **90**, 113508 (2007).
49. N. Wu, Q. Zhang, C. Zhu, D.S.H. Chan, M.F. Li, N. Balasubramanian, A. Chin, and D.L. Kwong: Alternative surface passivation on germanium for metal-oxide-semiconductor applications with high-*k* gate dielectric. *Appl. Phys. Lett.* **85**, 4127 (2004).
50. M. Houssa, G. Pourtois, B. Kaczer, B.D. Jaeger, F.E. Leys, D. Neils, K. Paredis, A. Vantomme, M. Caymax, M. Meuris, and M.M. Heyns: Experimental and theoretical study of Ge surface passivation. *Microelectron. Eng.* **84**, 2267 (2007).
51. N. Taoka, M. Harada, Y. Yamashita, T.T. Yamamoto, N. Sugiyama, and S.I. Takagi: Effects of Si passivation on Ge metal-insulator-semiconductor interface properties and inversion-layer hole mobility. *Appl. Phys. Lett.* **92**, 113511 (2008).
52. H.F. Ma, Z.H. Qin, M.C. Xu, D.X. Shi, H-J. Gao, S. Wang, and S.T. Pantelides: formation and evolution of a self-organized hierarchy of Ge nanostructures on Si(111)-(7 × 7): STM observations and first-principles calculations. *Phys. Rev. B: Condens. Matter Mater. Phys.* **75**, 165403 (2007).
53. A. Laha, H.J. Osten, and A. Fissel: Impact of Si substrate orientations on electrical properties of crystalline Gd_2O_3 thin films for high-*K* application. *Appl. Phys. Lett.* **89**, 143514 (2006).
54. J.E. Rowe and H. Ibach: Surface and bulk contributions to ultraviolet photoemission spectra of silicon. *Phys. Rev. Lett.* **32**, 421 (1974).
55. R.I.G. Uhrberg, G.V. Hansson, J.M. Nicholls, P.E.S. Persson, and S.A. Flodström: Photoemission study of the surface and bulk electronic structures of Si(111)7 × 7 and Si(111)$\sqrt{3} \times \sqrt{3}$:Al. *Phys. Rev. B: Condens. Matter Mater. Phys.* **31**, 3805 (1985).
56. J.A. Carlisle, T. Miller, and T-C. Chaing: Ge chemisorption and alloying on the Si(111)-(7 × 7) surface. *Phys. Rev. B: Condens. Matter Mater. Phys.* **49**, 13600 (1994).
57. P. Martensson, W.X. BNi, G.V. Hansson, J. Michael Nicholls, and B. Reihl: Surface electronic structure of Si(111)7 × 7-Ge and Si(111)5 × 5-Ge studied with photoemission and inverse photoemission. *Phys. Rev. B: Condens. Matter Mater. Phys.* **36**, 5974 (1987).
58. K. Kajiyama, Y. Tanishiro, and K. Takayanagi: Reconstructions and phase transitions of Ge on the Si(111)7 × 7 surface: I. Structural changes. *Surf. Sci.* **222**, 38 (1989).
59. Y.L. Wang, H-J. Gao, H.M. Guo, S. Wang, and S.T. Pantelides: Bonding configurations and collective patterns of Ge atoms adsorbed on Si(111)-(7 × 7). *Phys. Rev. Lett.* **94**, 106101 (2005).
60. M.C. Xu, H.F. Ma, W. Ji, B. Yang, and H-J. Gao: Growth of Ge hexagonal meshwork films on Si(111)-7 × 7. *Nanotechnology* **17**, 4413 (2006).
61. G. Pourtois, M. Houssa, B.D. Jaeger, B. Kaczer, F. Leys, M. Meuris, M. Caymax, G. Groeseneken, and M. Heyns: Threshold voltage shifts in Si passivated (100)Ge p-channel field effect transistors: Insights from first-principles modeling. *Appl. Phys. Lett.* **91**, 023506 (2007).
62. E. Fontes, J.R. Patel, and F. Comin: Direct measurement of the asymmetric dimer buckling of Ge on Si(001). *Phys. Rev. Lett.* **70**, 2790 (1993).
63. L. Patthey, F.L. Bullock, T. Abukawa, S. Kono, and L.S.O. Johansson: Mixed Ge–Si dimer growth at the Ge/Si(001)-(2 × 1) surface. *Phys. Rev. Lett.* **75**, 2538 (1995).
64. H. Oyanagi, K. Sakamoto, R. Shioda, Y. Kuwahara, and K. Haga: Ge overlayers on Si(001) studied by surface-extended X-ray-absorption fine structure. *Phys. Rev. B: Condens. Matter Mater. Phys.* **52**, 5824 (1995).
65. A. Laha, A. Fissel, and H.J. Osten: Effective control on flat band voltage of epitaxial lanthanide oxide based metal oxide semiconductor capacitors by interfacial carbon. *Appl. Phys. Lett.* **102**, 202902 (2013).
66. P. Shekhter, A. Roy Chaudhuri, A. Laha, S. Yehezkel, A. Shriki, H.J. Osten, and M. Eizenberg: The influence of carbon doping on the performance of Gd_2O_3 as high-*k* gate dielectric. *Appl. Phys. Lett.* **105**, 262901 (2014).
67. G. Bonnet, M. Lachkar, J.C. Colson, and J.P. Larpin: Characterization of thin solid films of rare earth oxides formed by the

Downloaded from https://www.cambridge.org/core. Technische Informationsbibliothek, on 05 Feb 2018 at 14:17:50, subject to the Cambridge Core terms of use, available at https://www.cambridge.org/core/terms. https://doi.org/10.1557/jmr.2017.22

metallo-organic chemical vapour deposition technique, for high temperature corrosion applications. *Thin Solid Films* **261**, 31 (1995).
68. T.M. Pan, X-C. Wu, and L-C. Yen: Effects of postdeposition annealing on physical and electrical properties of high-*k* Yb_2TiO_5 dielectrics. *J. Vac. Sci. Technol., A* **28**, 1084 (2010).
69. N. Umezawa, K. Shiraishi, T. Ohno, H. Watanabe, T. Chikyow, K. Torii, K. Yamabe, K. Yamada, H. Kitajima, and T. Arikado: First-principles studies of the intrinsic effect of nitrogen atoms on reduction in gate leakage current through Hf-based high-*k* dielectrics. *Appl. Phys. Lett.* **86**, 143507 (2005).
70. K. Seo, R. Sreenivasan, P. McIntyre, and K. Saraswat: Improvement in high-*k* (HfO_2/SiO_2) reliability by incorporation of fluorine. *IEEE Electron Device Lett.* **27**, 821 (2006).
71. C-H. Choi, S.J. Rhee, T.S. Jeon, N. Lu, J.H. Sim, R. Clark, M. Niwa, and D.L. Kwong: Thermally stable CVD HfO_xN_y advanced gate dielectrics with poly-Si gate electrode. In *Digest. International Electron Devices Meeting* (IEEE, Piscataway, 2002); p. 857.
72. X.P. Wanga, M.F. Lia, A. Chin, C.X. Zhu, J. Shao, W. Lu, X.C. Shen, X.F. Yu, R. Chi, C. Shen, A.C.H. Huan, J.S. Pan, A.Y. Du, P. Lo, D.S.H. Chan, and D.L. Kwong: Physical and electrical characteristics of high-κ gate dielectric $Hf_{(1-x)}La_xO_y$. *Solid-State Electron.* **50**, 986 (2006).
73. A. Roy Chaudhuri, A. Fissel, V.R. Archakam, and H.J. Osten: Improving dielectric properties of epitaxial Gd_2O_3 thin films on silicon by nitrogen doping. *Appl. Phys. Lett*. **102**, 022904 (2013).
74. A. Roy Chaudhuri, A. Fissel, and H.J. Osten: Investigation of band offsets and direct current leakage properties of nitrogen doped epitaxial Gd_2O_3 thin films on Si. *J. Appl. Phys.* **113**, 184108 (2013).
75. G. Dutta, K.P.S.S. Hembram, G. Mohan Rao, and U.V. Waghmare: Effects of O vacancies and C doping on dielectric properties of ZrO_2: A first-principles study. *Appl. Phys. Lett.* **89**, 202904 (2006).
76. K. Chu, J.P. Chang, M.L. Steigerwald, R.M. Flemimg, R.L. Opila, D.V. Lang, R.B. Van Dover, and C.D.W. Jones: Material and electrical characterization of carbon-doped Ta_2O_5 films for embedded dynamic random access memory applications. *J. Appl. Phys.* **91**, 308 (2002).
77. A. Laha, A. Bin, P.R.P. Babu, A. Fissel, and H.J. Osten: Enhanced electrical properties of carbon doped epitaxial Gd_2O_3 thin films on Si substrates. *ECS Trans.* **41**, 101 (2011).
78. G. Shang, P.W. Peacock, and J. Robertson: Stability and band offsets of nitrogenated high-dielectric-constant gate oxides. *Appl. Phys. Lett.* **84**, 106 (2004).
79. R. Gillen, S.J. Clark, and J. Robertson: Nature of the electronic band gap in lanthanide oxides. *Phys. Rev. B: Condens. Matter Mater. Phys.* **87**, 125116 (2013).
80. J. Robertson, K. Xiong, and S.J. Clark: Defect energy levels in high-*k* gate oxides. In *Defects in High-*k *Gate Dielectric Stacks NATO Science Series*, Vol. **220**, E. Gusev, ed. (Springer, The Netherlands, 2006); p. 175.
81. S. Guha and V. Naryan: Oxygen vacancies in high dielectric constant oxide-semiconductor films. *Phys. Rev. Lett.* **98**, 196101 (2007).
82. R.M. Fleming, D.V. Lang, C.D.W. Jones, M.L. Steigerwald, D.W. Murphy, G.B. Alers, Y-H. Wong, R.b. van Dover, J.R. Kwo, and A.M. Sergent: Defect dominated charge transport in amorphous Ta_2O_5 thin films. *J. Appl. Phys.* **88**, 850 (2000).
83. P. Broqvist and A. Pasquarello: Oxygen vacancy in monoclinic HfO_2: A consistent interpretation of trap assisted conduction, direct electron injection, and optical absorption experiments. *Appl. Phys. Lett.* **89**, 262904 (2006).
84. K. Xiong and J. Robertson: Oxygen vacancies in high dielectric constant oxides La_2O_3, Lu_2O_3, and $LaLuO_3$. *Appl. Phys. Lett.* **95**, 022903 (2009).
85. D. Liu, S.J. Clark, and J. Robertson: Oxygen vacancy levels and electron transport in Al_2O_3. *Appl. Phys. Lett.* **96**, 032905 (2010).
86. K. Tse, D. Liu, K. Xiong, and J. Robertson: Oxygen vacancies in high-*k* oxides. *Microelectron. Eng.* **84**, 2028 (2007).
87. R. Meyer, R. Liedtke, and R. Waser: Oxygen vacancy migration and time-dependent leakage current behavior of $Ba_{0.3}Sr_{0.7}TiO_3$ thin films. *Appl. Phys. Lett.* **86**, 112904 (2005).
88. J. Wang and S.T. McKinstry: Oxygen vacancy motion in Er-doped barium strontium titanate thin films. *Appl. Phys. Lett.* **89**, 172906 (2006).
89. H. Li and J. Robertson: Defect compensation in $LaAlO_3$ perovskite-based high dielectric constant oxides. *J. Appl. Phys.* **112**, 034108 (2012).
90. J. McPherson, J-Y. Kim, A. Shanware, and H. Mogul: Thermochemical description of dielectric breakdown in high dielectric constant materials. *Appl. Phys. Lett.* **82**, 2121 (2003).
91. J. McPherson, R.B. Khamankar, and A. Shanware: Complementary model for intrinsic time-dependent dielectric breakdown in SiO_2 dielectrics. *J. Appl. Phys.* **88**, 5351 (2000).

Downloaded from https://www.cambridge.org/core. Technische Informationsbibliothek, on 05 Feb 2018 at 14:17:20, subject to the Cambridge Core terms of use, available at https://www.cambridge.org/core/terms. https://doi.org/10.1557/jmr.2017.22